



OPEN ACCESS

EDITED BY

ZhaoYang Dong,
City University of Hong Kong, Hong
Kong SAR, China

REVIEWED BY

Minh Quan Duong,
University of Science and Technology,
The University of Danang, Vietnam
Hossein Lotfi,
Hakim Sabzevari University, Iran

*CORRESPONDENCE

G. M. Shafiullah,
✉ GM.Shafiullah@murdoch.edu.au
Shameem Ahmad,
✉ shameem.ahmad@bracu.ac.bd

RECEIVED 28 October 2025

REVISED 18 January 2026

ACCEPTED 24 February 2026

PUBLISHED 08 April 2026

CITATION

Talha MA, Ahmad S, Mannan MA,
Hazari MR, Ahmed T, Huda ASN, and
Shafiullah GM (2026) Adaptive
distribution network reconfiguration
with renewable energy and EV
integration using reverse-multiverse
learning archimedes algorithm.
Front. Energy Res. 14:1731439.
doi: 10.3389/fenrg.2026.1731439

COPYRIGHT

© 2026 Talha, Ahmad, Mannan, Hazari,
Ahmed, Huda and Shafiullah. This is an
open-access article distributed under
the terms of the [Creative Commons
Attribution License \(CC BY\)](https://creativecommons.org/licenses/by/4.0/). The use,
distribution or reproduction in other
forums is permitted, provided the
original author(s) and the copyright
owner(s) are credited and that the
original publication in this journal is
cited, in accordance with accepted
academic practice. No use, distribution
or reproduction is permitted which
does not comply with these terms.

Adaptive distribution network reconfiguration with renewable energy and EV integration using reverse-multiverse learning archimedes algorithm

Md Abu Talha¹, Shameem Ahmad^{2*},
Mohammad Abdul Mannan¹, Md. Rifat Hazari¹, Tofael Ahmed³,
A. S. Nazmul Huda² and G. M. Shafiullah^{4*}

¹Department of Electrical and Electronic Engineering, Faculty of Engineering, American International University–Bangladesh, Dhaka, Bangladesh, ²Department of Electrical and Electronic Engineering, BSRM School of Engineering, BRAC University, Dhaka, Bangladesh, ³Department of Electrical and Electronic Engineering, Chittagong University of Engineering & Technology, Chattogram, Bangladesh, ⁴School of Engineering and Energy, College of Science, Technology, Engineering and Mathematics, Murdoch University, Perth, WA, Australia

The increasing integration of renewable energy sources (RES) and the widespread adoption of electric vehicles (EVs) have significantly expanded distribution networks in recent years, leading to challenges such as increased power losses and reduced transmission reliability. To address these issues, optimizing distribution network topology through reconfiguration is crucial for enhancing voltage stability and improving overall system performance. This paper presents an optimized distribution network reconfiguration (DNR) model that incorporates RES and EVs, focusing on the optimal placement of bus tie switches and reactive power regulation using the Reverse-Multiverse Learning Archimedes Algorithm (RMLAA). The main goals are to minimize power losses and voltage deviations across buses, while optimizing reconfiguration and reactive power from RES (wind and PV) and EVs, with RMLAA proposed as the decision variable. The RMLAA integrates Reverse-learning and Multiverse-directing strategies to enhance optimization precision and computational efficiency in multi-objective optimization. It focuses on minimizing reactive and active power losses while improving voltage stability. To assess its effectiveness, the RMLAA is compared with widely used algorithms, including Genetic Algorithms (GA), Particle Swarm Optimization (PSO), and Harris Hawks Optimization (HHO), using the CEC'17 benchmark test suite. Applied to the IEEE 33-bus and 69-bus systems, the RMLAA achieves remarkable reductions in active power losses of 70.35% and 69.08%, and in reactive power losses of 47.65% and 26.01%, respectively. Additionally, voltage stability improves by 15.2%, and computational efficiency increases by up to 22.3% compared to conventional methods. The study further demonstrates the effectiveness of the proposed algorithm through a comparative analysis with existing algorithms on the IEEE 33-bus and 69-bus systems. These findings confirm that the proposed RMLAA-based DNR framework is an effective and

robust approach for improving efficiency, voltage stability, and computational performance in modern distribution networks with RES and EV integration.

KEYWORDS

Archimedes optimization algorithm, distribution network reconfiguration, electrical vehicles, power loss minimization, reactive power optimization, renewable energy resources, voltage stability

1 Introduction

The transition to renewable energy is essential for reducing greenhouse gas emissions and promoting a sustainable energy future. According to the International Renewable Energy Agency (IRENA), global installed capacity reached 9.0 TW by 2023, with renewable energy sources accounting for 43.0% and non-renewable sources for 50.4% (IRENA, 2024). The integration of electric vehicles (EVs) introduces load variability and, when combined with the intermittent nature of renewable sources like solar and wind, necessitates advanced grid management and energy storage solutions (Abdelsattar et al., 2024). Distributed Energy Resources (DERs) are instrumental in meeting load demands near load centers, optimizing network performance by reducing power losses, enhancing voltage stability, and improving reliability (Fose et al., 2024).

The incorporation of EVs and RES brings forth notable challenges and opportunities for enhancing the performance of distribution networks. A primary focus area is the optimization of reactive power, with methods such as second-order cone programming demonstrating effectiveness, particularly in systems like the IEEE 33-bus network (Liu and Gao, 2023). To tackle the variability of renewable energy, strong models for distributed generation (DG), along with network reconfiguration, offer solutions to address the difficulties associated with renewable integration (Jin et al., 2023). Multi-objective strategies, including those employing Adaptive Particle Swarm Optimization (APSO) and Teaching-Learning-Based Optimization (TLBO), aim to balance technical, economic, and environmental considerations in the planning of solar distributed generation and DSTATCOM alongside network reconfiguration (Saw et al., 2023). The strategic placement of EV charging stations is essential for maintaining cost efficiency and ensuring stable operations within the network (Subramaniam and Singh, 2023), while managing the voltage of distributed photovoltaic clusters is crucial for alleviating uneven voltage distribution and minimizing network losses (Yang et al., 2023). To enhance sustainability, low-carbon dispatching methods based on carbon emission flow theory have been used to optimize environmental impact in distribution systems (Pirouzi et al., 2020), and hybrid strategies combining electric-thermal flows and carbon trading mechanisms have demonstrated improved system performance (Karimi et al., 2019). Energy storage systems also play a critical role in optimizing grid stability and operational efficiency, with methods like the improved BAT algorithm offering effective storage allocation (Monteiro et al., 2020). The incorporation of EVs with Vehicle-to-Grid (V2G) technology supports voltage regulation and reactive power management in distribution networks (Mazumder

and Debbarma, 2020). Multi-objective techno-economic frameworks, integrating reactive power support from battery storage systems, balance technical performance and economic feasibility (Rawat et al., 2021).

Advanced optimization techniques have been employed to enhance network reconfiguration and DG allocation. The Archimedes Optimization Algorithm (AOA) has been successfully applied for optimal allocation of distributed generations, capacitor banks, and voltage regulators, addressing active and reactive power compensation (Cai and Zhao, 2023). Similarly, the Battle Royale Optimization (BRO) algorithm has been explored for the optimal integration of EVs and distributed generations in distribution networks (Rao et al., 2023). Mixed-integer linear programming (MILP) models have been developed for simultaneous network reconfiguration and optimal capacitor placement, contributing to improved system performance (Emimal and Mahiban, 2023; Mahmoud et al., 2021; Habib et al., 2022). Binary Particle Swarm Optimization (BPSO) has also been applied to enhance the performance of reconfigured networks, particularly for integrating photovoltaic systems and energy storage (Gallego et al., 2022). Home energy management strategies have been optimized using meta-heuristic algorithms, especially under time-of-use (TOU) tariffs, to reduce energy costs (Liemthong et al., 2022). Studies have further compared grid reactive voltage regulation with distribution feeder reconfiguration to accommodate growing EV penetration, identifying strengths and limitations in both approaches (Nagi et al., 2022). Research efforts have provided diverse insights into Distribution Network Reconfiguration (DNR) and its optimization. In 2011, the harmony search algorithm (HSA) was employed to solve the DNR problem, although it was found that the penalty coefficients of the fitness function in HSA are challenging to handle (Rao et al., 2011). A new formulation introduced in (Castro et al., 2024) focused on optimal radial topologies, though it increased computational time without significant benefits. Mixed-integer non-linear programming (MINLP) was utilized for DNR in (Jabr et al., 2012), showing comparable results to mixed-integer linear programming (MILP), but with additional mathematical complexity due to quadratic constraints. Quadratic programming (QP) and quadratically constrained programming (QCP) have been employed to model DNR problems, adding constraints related to maximum complex power (Taylor and Hover, 2012). Another approach using MILP with piecewise linear approximations for power losses was proposed in (Llorens-Iborra et al., 2012), although performance degraded in highly non-linear DSR problems. Improvements over these models were seen in (Ferdavani et al., 2013), where the neighbor-chain updating process (NCUP) replaced Branch Exchange (BE), leading to better solutions. Graph theory-based approaches for radiality constraints, modeled as spanning tree problems, have

shown promise in reconfiguration times for planar networks but not for non-planar ones (Ahmadi and Martí, 2015a). In Ahmadi and Martí (2015b), linear current flow equations were proposed to reduce losses using MILP and MIQCP, while a binary convex model presented in (Hijazi and Thiébaux, 2015) demonstrated quicker results for large systems, although it was more computationally intensive for medium-sized networks. Various algorithms have been suggested for optimizing radial distribution networks, including Chaotic Particle Swarm Chicken Swarm Fusion Optimization (CPSCSFO) (Wu et al., 2023), a Hybrid Genetic Algorithm combined with K-Nearest Neighbors (Jo et al., 2024), and a method for Joint Distributed Generation Maximization and Radial Distribution Network Reconfiguration (So et al., 2022). Furthermore, multi-objective stochastic frameworks have been created for the allocation of wind energy resources in unbalanced distribution networks to tackle uncertainties in load and wind power distribution (Duan et al., 2024). Various heuristic methods (Jasthi and Das, 2018), including simulated annealing (SA) (Esmailian and Fadaeinedjad, 2015), modified Tabu Search (MTS) (Abdelaziz et al., 2010), Modified Plant Growth Simulation Algorithm (MPGSA) (Rajaram et al., 2015), Adaptive Ant Colony Optimization (AACO) (Esmailian and Fadaeinedjad, 2015; Saffar et al., 2011; Swarnkar et al., 2011; Abdelaziz et al., 2012), and others such as Data-driven teaching-learning-based optimization (DTLBO) (Lotfipour and Afrakhte, 2016), Binary GA (BGA) (Sahoo and Prasad, 2006), Minimum-Current Circular-Updating-Mechanism (MCCUM) (Zin et al., 2012), Barnacle Growth Algorithm (BGA) (Taher and Karimi, 2014), Fast Nondominated Sorting Genetic Algorithm (FNSGA) (Eldurssi and O'Connell, 2015), and Dragonfly Algorithm (DFA) (Reddy and Reddy, 2016), continue to drive progress in this field. Researchers are actively working on methods like Whale Optimization Algorithm (IWOA) to minimize energy not supplied (ENS) and operational costs (Lotfi et al., 2025). Other approaches focus on optimizing the placement of EVCS, PVUs, and CAPBs to reduce losses and enhance grid stability (Duong et al., 2025), and use bi-level optimization with disconnecter and TCLBS switches for improved reliability during peak demand (Parsadust et al., 2025). Additionally, dynamic reconfiguration strategies are being developed to manage load imbalances (Lotfi, 2025). Table 1, presents a summary of the literature review along with key paper contributions.

Despite advancements in DNR and optimization techniques, key challenges remain. The limitations identified from the above literature review are as follows:

- Existing methods struggle to handle the variability and uncertainty introduced by renewable energy sources like solar and wind power, and electric vehicle loads.
- Many existing optimization frameworks do not comprehensively address both active and reactive power flows, which are crucial for maintaining voltage stability and minimizing power losses.
- Current algorithms often face limitations in scalability and computational efficiency when applied to large-scale networks, leading to longer computation times and suboptimal solutions.
- Handling multi-objective constraints effectively remains a challenge. Existing approaches do not consistently optimize

multiple objectives such as power loss reduction, voltage profile improvement, and reactive power management simultaneously.

This study presents the Reverse-Multiverse Learning Archimedes Algorithm (RMLAA), enhanced with reverse learning and a multiverse-directing strategy, to address modern DNR limitations from the above literature. These enhancements improve the algorithm's efficiency in managing the variability of RES and dynamic EV loads by optimizing active and reactive power flows with higher scalability, faster computation, and higher accuracy. Reverse learning diversifies search exploration by generating mirrored solutions within defined boundaries, effectively avoiding local optima, while the multiverse-directing mechanism introduces varied exploration paths, enabling comprehensive searches across solution spaces. Together, these strategies optimize network configurations by dynamically altering tie-switch statuses and regulating reactive power contributions from RES and EVs, ensuring robust and efficient network performance. Applied to the IEEE 33-bus and 69-bus systems, the algorithm integrates switch reconfiguration and reactive power management to improve voltage profiles, minimize power losses, and ensure stable network performance.

The main contributions are outlined as follows:

- The Reverse-Multiverse Learning Archimedes Algorithm (RMLAA) is introduced, which enhances the original AOA by adding reverse learning and a multiverse-directing mechanism. The algorithm is assessed using the CEC17 benchmark test suite and compared with popular algorithms like GA, HHO, and PSO.
- A multi-objective Distribution Network Reconfiguration (DNR) model is proposed that integrates renewable energy sources (RES) and electric vehicles (EVs), aiming to improve voltage profiles and reduce power losses. The model, applied to modified IEEE 33-bus and 69-bus systems, uses RMLAA for network reconfiguration with RES and EV integration.
- An optimization framework has been developed to reduce reactive power losses, focusing on how renewable energy sources (RES) like wind and photovoltaic (PV) systems, as well as electric vehicles (EVs), contribute to reactive power. Using the RMLAA method, this approach manages reactive power to help maintain voltage stability and boost the operational efficiency of distribution networks.

The structure of this paper is as follows: Section 2 presents the mathematical formulation for DNR, focusing on minimizing power losses and voltage deviations, with constraints applied to the IEEE 33-bus and 69-bus systems, integrating renewable energy and EVs. Section 3 introduces the RMLAA, highlighting its enhancements over the original AOA and comparing it to algorithms like GA, HHO, and PSO regarding computation efficiency. Section 4 provides a performance comparison using the IEEE test systems, demonstrating RMLAA's effectiveness. Section 5 concludes with key findings and suggestions for future research, including scaling and real-time applications.

TABLE 1 Summary of literature review and key paper contributions.

Ref.	Methods	Power loss	Voltage deviation	Optimization reactive power	Tested on IEEE system	Integration		Limitation
						RES	EVs	
Liu and Gao (2023)	SOCP	✓	✓	✓	33-Bus	✓	x	High computational complexity for large systems
Jin et al. (2023)	Bi-LRO	✓	✓	✓	33 and 69-bus	✓	x	Limited scalability to larger or highly meshed networks
Saw et al. (2023)	APSO, TLBO	✓	✓	✓	69-Bus	✓	x	May converge to local optima in some scenarios
Subramaniam and Singh (2023)	AT-AQ, AO, ASO	✓	x	✓	Generic RDS	✓	✓	Lack of detailed comparison with other optimization methods
Alshareef and Fathy (2023)	ROA	✓	✓	✓	33 and 69-bus	✓	✓	Performance is sensitive to parameter tuning
Yang et al. (2023)	PSO-BP	✓	✓	✓	33-Bus	✓	x	Requires substantial computational resources for large systems
Pirouzi et al. (2020)	MILP	✓	✓	✓	33-Bus	x	✓	Cannot handle non-linear constraints effectively
Karimi et al. (2019)	KHA	✓	x	✓	33-Bus	✓	x	Convergence speed is slow in certain cases
Monteiro et al. (2020)	BPSO, ANN	✓	✓	✓	37-Bus	✓	x	Accuracy highly depends on training data quality in ANN.
Mazumder and Debbarma (2020)	WCA	✓	✓	✓	33-Bus	x	✓	Struggles to maintain balance between exploration and exploitation
Rawat et al. (2021)	NCMILP	✓	✓	✓	33-Bus	✓	x	Complexity increases with additional renewable energy sources
Cai and Zhao (2023)	AOA	✓	✓	✓	-	✓	x	Limited application to real-time scenarios
Rao et al. (2023)	INBA	✓	✓	✓	33-Bus	✓	x	Requires more rigorous validation with different systems

(Continued)

TABLE 1 Continued

Ref.	Methods	Power loss	Voltage deviation	Optimization reactive power	Tested on IEEE system	Integration		Limitation
						RES	EVs	
Emimal and Mahiban (2023)	IIFFTA, SOS	✓	x	✓	69-Bus	✓	✓	Partial effectiveness in systems with high renewable penetration
Mahmoud et al. (2021)	AOA	✓	✓	✓	TDRF, Egypt	✓	x	Limited implementation details for generic usage
Habib et al. (2022)	BRO, GA, PSO, APSO	✓	✓	✓	CIGRE 14-bus	✓	✓	High reliance on initial parameter settings
Gallego et al. (2022)	MILP	✓	✓	✓	33 and 69-bus	x	x	Non-linear relationships are approximated, reducing accuracy
Liemthong et al. (2022)	Meta-heuristic	✓	x	x	HEMS	✓	✓	Limited exploration of optimization space
Nagi et al. (2022)	MST, GA, MILP	✓	✓	✓	33-Bus	x	✓	Complex implementation due to hybrid methods
Hijazi and Thiébaux (2015)	MINLP, SDP	✓	✓	✓	32 and 70-bus	✓	x	Requires significant computational resources for large systems
Wu et al. (2023)	CPSCSFO		✓	✓	33-Bus	✓	x	Poor scalability for highly meshed networks
Jo et al. (2024)	HGA, KNN	✓	✓	✓	123-Bus	✓	x	Overfitting risks with machine learning-based approaches
So et al. (2022)	MIP	✓	✓	✓	33-Bus	✓	x	Unable to fully capture uncertainties in renewable integration
Duan et al. (2024)	IDO	✓	✓	✓	33-Bus	✓	x	Tends to converge prematurely in complex systems
Jasthi and Das (2018)	Heuristic	✓	✓	✓	33-Bus	✓	x	Results depend on the quality of heuristic rules defined
Esmacilian and Fadaeinedjad (2015)	ACO, HAS, HBMO	✓	✓	✓	33-Bus	✓	x	Risk of getting stuck in local optima due to limited global search capability

2 Mathematical formulation for DNR

DNR enhances power distribution network efficiency and reliability by adjusting tie and sectionalizing switches open/close status. This minimizes power losses, improves voltage profiles, and simplifies the network topology, ensuring connectivity under varying load conditions. Strategic reconfiguration enables adaptation to scenarios like faults and maintenance activities (Morsy et al., 2022), making DNR crucial for modern power systems, especially with the growing integration of RES and EVs, which introduce variability and uncertainty (Youssef, 2021). By optimizing network configurations, DNR helps maintain stability and performance in the face of operational challenges such as voltage fluctuations, power losses, and load imbalances (Hizarci et al., 2022).

2.1 Objective function

The primary objective of the DNR model is to minimize active power loss and voltage deviation and optimize reactive power within the power distribution network, ensuring efficient, stable, and reliable operations. Active power loss primarily results from the resistance of electrical conductors, and reducing this loss enhances the network's overall efficiency. The objective function for minimizing active power loss can be expressed as Equation 1.

$$f_1 = \min(P_{loss}) = \sum_{l=1}^{N_l} r_l \frac{P_l^2 + Q_l^2}{U_l^2} \quad (1)$$

Where N_l represents the set of all branches, r_l is the resistance of branch l , P_l and Q_l are the active and reactive power flow, and U_l is the voltage at node i . By optimizing network configuration, power can be delivered more efficiently, reducing both energy waste and operational costs (Pan et al., 2022).

In addition to minimizing power loss, the model also targets voltage deviation, which refers to the difference between the actual voltage at a node and its rated value. Voltage deviations can lead to power quality issues that affect the performance and lifespan of electrical equipment. The objective function for minimizing voltage deviation can be formulated as Equation 2:

$$f_2 = \min(V_d) = \sum_{j \in N_i} (V_j - V_j^*)^2 \quad (2)$$

Where V_j is the actual voltage at node j , V_j^* is the rated voltage, and N_i is the set of nodes in the network (Arulprak et al., 2021). Reducing voltage deviations helps maintain network stability, ensures a reliable power supply, and prevents harmful over- or under-voltage conditions.

The third objective of the model is to optimize reactive power, which is essential for maintaining voltage levels and improving power quality throughout the network. The equation for minimizing reactive power mismatch is provided in Equation 3.

$$f_3 = \min(Q_{loss}) = \sum_{k=1}^{N_k} (Q_k - Q_k^*)^2 \quad (3)$$

Where Q_k is the reactive power at node k , and Q_k^* is the desired reactive power at that node (Tran et al., 2020). Optimizing reactive power improves voltage stability, reduces power losses, and ensures more efficient use of the network's resources. Together, these three

objectives minimizing power loss, minimizing voltage deviation, and optimizing reactive power create a comprehensive optimization framework for DNR that enhances the performance and reliability of modern power distribution networks.

The multi-objective function combining active power loss, voltage deviation, and reactive power mismatch is expressed in Equation 4.

$$\min f_{multi} = \lambda_1 f_1 + \lambda_2 f_2 + \lambda_3 f_3 \quad (4)$$

Subject to:

- Equality Constraints:

The equality constraint for the network is defined in Equation 5.

$$\sum_{l=1}^{N_l} P_l - \sum_{k=1}^{N_k} Q_k = 0 \quad (5)$$

- Inequality Constraints:

The inequality constraints are outlined in Equation 6.

$$\begin{cases} V_{min} \leq V_j \leq V_{max}, \forall j \in N_l \\ P_{min} \leq P_l \leq P_{max}, \forall l \in N_l \\ Q_{min} \leq Q_k \leq Q_{max}, \forall k \in N_k \\ r_l \cdot \left(\frac{P_l^2 + Q_l^2}{U_l^2} \right) \leq r_{max}, \forall l \in N_l \end{cases} \quad (6)$$

Where, $\lambda_1, \lambda_2, \lambda_3$ are the weights assigned to the respective objective functions f_1, f_2, f_3 .

2.2 Constraint conditions

The optimization problem for DNR must satisfy several constraints that reflect the physical and operational limitations of the network, ensuring practical and feasible solutions. The first set of constraints consists of the active and reactive power flow equations, which serve as equality constraints in the optimization problem. These equations ensure power balance by defining the relationship between power flow, voltage magnitudes, and phase angles. The active and reactive power flow between nodes i and j can be expressed using Equations 7, 8 respectively.

$$P_{ij} = \frac{V_i V_j}{X_{ij}} \sin(\theta_i - \theta_j) \quad (7)$$

$$Q_{ij} = \frac{V_i^2}{X_{ij}} - \frac{V_i V_j}{X_{ij}} \cos(\theta_i - \theta_j) \quad (8)$$

Where P_{ij} and Q_{ij} represent the active and reactive power flow between nodes i and j , V_i and V_j are the voltage magnitudes at nodes i and j , X_{ij} is the reactance of the line, and θ_i and θ_j are the voltage phase angles at nodes i and j .

The power balance constraints ensure that the total generation equals the total demand plus losses, maintaining network stability. The active and reactive power balance can be expressed using Equations 9, 10 respectively.

$$P_{slack} + \sum_{j=1}^{N_{DG}} P_{DG,j} = \sum_{j=1}^{N_{th}} P_{D,j} + \sum_{j=1}^{N_{br}} P_{l,j} \quad (9)$$

$$Q_{slack} + \sum_{j=1}^{N_{DG}} Q_{DG,j} = \sum_{j=1}^{N_{th}} Q_{D,j} + \sum_{j=1}^{N_{br}} Q_{l,j} \quad (10)$$

In these equations, P_{slack} and Q_{slack} are the active and reactive power from the slack bus, $P_{DG,j}$ and $Q_{DG,j}$ are the active and reactive power outputs of distributed generators, and $P_{D,j}$ and $Q_{D,j}$ are the active and reactive power demands at the j th node. These constraints ensure that the power generated matches the power consumed plus the losses, maintaining system stability and preventing issues like overloading or voltage instability (Tran et al., 2020).

Voltage, current, and switching constraints further ensure the safe and efficient operation of the network. The voltage at each bus must remain within specified limits at the k th node as shown in Equation 11 to maintain power quality and prevent equipment damage:

$$V_{k,min} \leq V_k \leq V_{k,max} \quad (11)$$

Each branch current must also be constrained within safe limits as shown in Equation 12 to avoid thermal overload and damage:

$$0 \leq I_m \leq I_{m,max}, m = 1, 2, 3, \dots, N_{br} \quad (12)$$

Finally, only one switch status change is allowed per loop during reconfiguration, ensuring the network remains connected and operational. The switching constraint to ensure radial operation are defined in Equation 13.

$$N_{um,m} = 1, n = 1, 2, 3, \dots, loop_{max} \quad (13)$$

These constraints ensure that the network remains balanced, operational, and within safe voltage and current limits during reconfiguration, preventing service interruptions and maintaining reliability.

2.3 Reactive power regulation of wind power, PV, and EVs

Reactive power regulation is crucial for maintaining voltage stability and power quality in networks with wind power, PV systems, and EVs. Constraints ensure these sources operate within their reactive power limits, supporting efficient power distribution. Proper management enhances network stability, with EVs becoming increasingly important as their integration grows.

2.3.1 Reactive power control for wind turbines

The wind turbine system uses a doubly-fed induction generator (DFIG), adapted from (Yang et al., 2017) and converts mechanical energy from the turbine into electrical energy and then supplied to the grid through both the stator and rotor of the DFIG, utilizing a back-to-back converter system composed of a rotor-side converter and a grid-side converter to manage the flow of electricity. The reactive power regulation model for wind power involves several key components and equations. At the core, the input mechanical power (P_m) captured by the wind turbine is directly related to the wind speed and is given by the Equation 14 and the tip speed ratio of the wind turbine can be expressed as Equation 15 (Yang et al., 2017).

$$P_m = \frac{1}{2} C_p \rho \pi R^2 V^3 \quad (14)$$

$$\lambda = \frac{\omega_m R}{V} \quad (15)$$

Where ρ is the air density, R is the radius of the wind turbine, V is the wind speed, C_p is the power coefficient, λ is blade tip speed ratio, and ω_m representing the turbine's rotation speed. The active power (P_w) generated by the turbine is managed through maximum power point tracking (MPPT) and depends on the wind speed (s_w) relative to cut-in (s_{in}), and cut-out (s_{out}) wind speeds. P_{base} and S_{base} are the rated output power and rated wind speed, respectively. The active power generated by wind turbine under MPPT can be expressed Equation 16.

$$P_w = \begin{cases} 0; & (s_w \leq s_{in} \text{ or } s_w \geq s_{out}) \\ P_{base} \left(\frac{s_w - s_{in}}{s_{base} - s_{in}} \right); & (s_{in} \leq s_w < s_{base}) \\ P_{base}; & (s_{base} \leq s_w < s_{out}) \end{cases} \quad (16)$$

Reactive power (Q_w) supplied to the grid is a combination of contributions from the stator (Q_{stator}) and the grid-side ($Q_{converter}$) converter, bounded by maximum ($Q_{w,max}$) and minimum ($Q_{w,min}$) limits. The inverter's reactive power capability can be expressed as Equation 17.

$$Q_w = Q_{stator} + Q_{converter} \quad (17)$$

The reactive power limits for wind turbine can be presented using Equation 18.

$$Q_{w,min} \leq Q_w \leq Q_{w,max} \quad (18)$$

Where,

$$Q_{w,max} = Q_{stator,max} + Q_{converter,max}, \text{ and } Q_{w,min} = Q_{stator,min} + Q_{converter,min}$$

2.3.2 Photovoltaic system reactive power management

The performance of small-scale photovoltaic systems is affected by several environmental factors, including solar irradiation and temperature, which directly impact a PV system's active power output (P_{pv}) (Elymany et al., 2024). It can be calculated using the MPPT principle in the ideal state using Equation 19.

$$P_{pv} = P_{base,pv} \frac{S_{pv}}{1000} [1 + \alpha_{pv}(T - T_{ref})] \quad (19)$$

Where, $P_{base,pv}$ represents the rated total power of the PV system connected to the distribution network. The temperature conversion coefficient is denoted by α_{pv} , while T indicates the current temperature at the recording time. The reference temperature value is symbolized by T_{ref} , and the solar irradiation at the current time is represented by s_{pv} . The reactive power output (Q_{pv}) of a PV system is limited by the capacity of the PV inverter (S_{pv}) and the active power output (P_{pv}). The upper ($Q_{pv,max}$) and lower bounds ($Q_{pv,min}$) of the reactive power output is expressed by Equation 20.

$$Q_{pv,min} \leq Q_{pv} \leq Q_{pv,max} \quad (20)$$

Where,

$$Q_{pv,max} = \left(\sqrt{S_{pv}^2 - P_{pv}^2} \right), \text{ and } Q_{pv,min} = - \left(\sqrt{S_{pv}^2 - P_{pv}^2} \right)$$

2.3.3 Electric vehicle reactive power contribution

Electric vehicles (EVs) act as integrated energy storage systems, with their charging station converters offering precise control over active and reactive power, thereby contributing to reactive power optimization in distribution networks. The charging process involves converting three-phase AC into DC, enabling bidirectional power flow where EVs can either supply excess energy to the grid or receive power for charging when necessary (Jiménez et al., 2024). The active power (P_{EV}) of an EV can be described by Equation 21 (Jiménez et al., 2024):

$$P_{EV} = \frac{V_c V_s \sin(\theta)}{\omega L_c} \quad (21)$$

The grid voltage, denoted as V_s , interacts with the voltage of the EV charging piles, represented as V_c . The phase difference between these two voltages is indicated by θ . Additionally, the angular frequency of the AC system is symbolized by ω . The total interface inductance, which encompasses both the line inductance and the charger filter inductance between the charger and the grid, is denoted as L_c . The reactive power (Q_{EV}) of an EV is limited by the capacity of the converters in the charging piles (S_{EV}). The upper ($Q_{EV,max}$) and lower ($Q_{EV,min}$) bounds of the reactive power regulation range can be presented by Equation 22.

$$Q_{EV,min} \leq Q_{EV} \leq Q_{EV,max} \quad (22)$$

Where,

$$Q_{EV,max} = \left(\sqrt{S_{EV}^2 - P_{EV}^2} \right), \text{ and } Q_{EV,min} = -\left(\sqrt{S_{EV}^2 - P_{EV}^2} \right)$$

2.4 Network configuration settings

The study evaluates several algorithms for DNR using the IEEE 33-bus and 69-bus systems, which consist of five loops with distributed switches, as shown in Figures 1a,b. Changeable switches serve as decision variables, with regulation resources including wind turbines, PV systems, and EVs, whose reactive power is controlled via grid-side and charging pile inverters. The 33-bus system includes 4-PV systems, 3-wind turbines, and 3-EV stations with inverter capacities of 0.25 MW (PV system) and 0.28 MW (EV), while the 69-bus system has 8-PV systems, 6-wind turbines, and 6-EV stations with 30 kW inverters. The active power injected into the distribution network from renewable energy sources is influenced by local climatic factors. Solar irradiation significantly affects PV systems, while wind speed is crucial for wind turbine generation. Identifying specific buses for renewable energy or EV connections is crucial. The selected locations of PV, wind, and EV connections are determined based on their best performance, ensuring stability and strengthening the weakest bus to maintain overall system stability. The best PV bus locations and corresponding sizes in kW are 12 kW (2), 14 kW (4), 16 kW (7), and 18 kW (8) for the 33-bus system, and 6 kW (7), 9 kW (8), 12 kW (17), 15 kW (18), 18 kW (21), 21 kW (59), 24 kW (62), and 27 kW (65) for the 69-bus system. Similarly, the best wind bus locations and corresponding sizes in kW are 200 kW (29), 266 kW (30), and 300 kW (31) for the 33-bus system, and 33.31 kW (11), 100.00 kW (12), 166.66 kW (49), 233.00 kW (50), 300.00 kW (61), and 299.99 kW (64) for the 69-bus

system. With charge or discharge states, EVs can significantly alter active power output, but as shown in Equation 22, the sign of active power does not impact the reactive power regulation range. Table 2, presents the systematic distribution of switches across different loops to facilitate network reconfiguration. The switch allocation was determined to ensure even distribution while avoiding redundancy. As a result, the reconfigurable switches were selected within five distinct loops, serving as key decision variables for optimization.

2.4.1 IEEE 33-bus system with PV, wind turbine, and EVs

In the 33-bus system, the PV systems are connected to nodes 2, 4, 7, and 8, with solar irradiances between 600 and 900 W/m². Their active power outputs range from 12 to 18 kW, and their reactive capacities vary from ±21.90 to ±17.31 kVAR. Wind turbines are connected to nodes 29, 30, and 31, with 9–13 m/s wind speeds, active power outputs from 200 to 300 kW, and reactive capacities between –136.60, and 151.11 kVAR. EV power stations are connected to nodes 24, 25, and 32, with active power outputs from 156.74 to 177.85 kW, and reactive capacities between ±209.33 and ±211.43 kVAR. These integrations, shown in Figure 2, help optimize power flows and voltage stability, with detailed system parameters in Table 3.

2.4.2 IEEE 69-bus system with PV, wind turbine, and EVs

Photovoltaic (PV) systems in the 69-bus network are installed at nodes 7, 8, 17, 18, 21, 59, 62, and 65, where solar irradiance ranges between 350 and 1350 W/m². The active power output of these units spans from 6.00 to 27.00 kW, while their reactive capacity ranges between +29.19 and –13.11 kVAR. Wind turbines at nodes 11, 12, 49, 50, 61, and 64 operate at 4–14 m/s wind speeds, producing 33.31–300.00 kW active power and ±41.29 to ±17.40 kVAR reactive capacity. EV power stations are installed at nodes 9, 16, 45, 46, 51, and 69, providing active power outputs ranging from 16.44 kW to 22.85 kW. At node 46, a value of –19.97 kW indicates that EV charging is occurring. The reactive capacity at this station varies between approximately –19.81 kVAR and +24.94 kVAR. These distribution and parameter settings highlight the precision needed to manage reactive power and maintain stable network operations with new energy sources and EVs. As shown in Figure 3, these integrations optimize power flows and voltage stability; system parameters are listed in Table 4.

3 Proposed reverse-multiverse learning Archimedes algorithm (RMLAA) for DNR

Initialize a population of candidate DNR solutions, each representing different switch configurations. Also, set the volume (V), density (D), and acceleration (A) for each solution to calculate buoyant force and movement, following the Archimedes principle (Hashim et al., 2020). The Archimedes Optimization Algorithm (AOA) uses volume, density, and buoyant force to find optimal solutions. Candidate solutions are initialized, buoyant forces are calculated, and positions are updated until the best

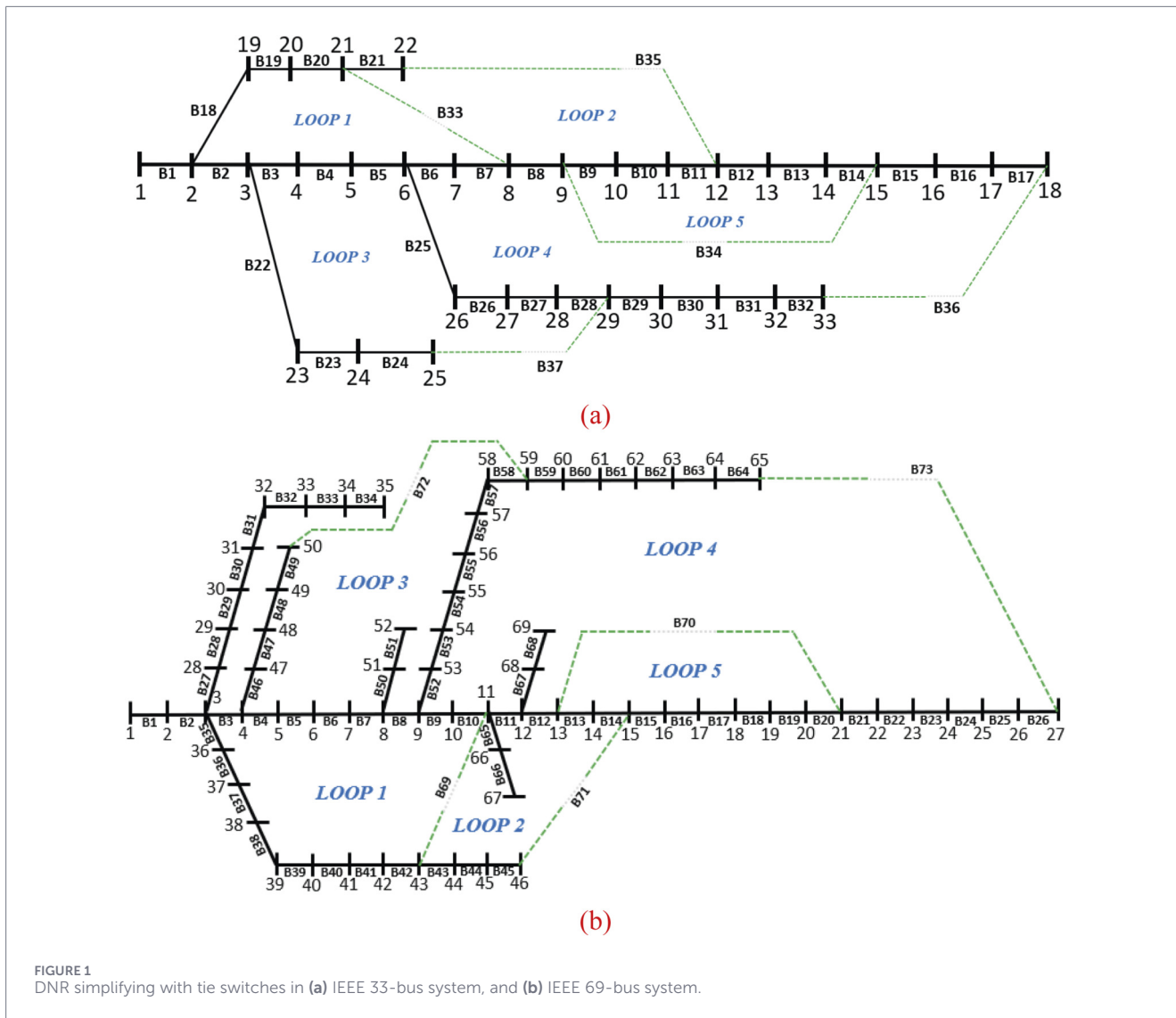


FIGURE 1 DNR simplifying with tie switches in (a) IEEE 33-bus system, and (b) IEEE 69-bus system.

TABLE 2 Different loops of switches for DNR.

Loops	Switches	
	33-Bus system	69-Bus system
1	2,3,4,5,6,7,18,19,20	3,35,36,37,38,39,40,41,42,69
2	8,9,10,11,21,33,35	43,44,45,71
3	22,23,24,25,26,27,28,37	13,14,15,16,17,18,19,20,70
4	15,16,17,29,30,31,32,36	4,5,6,7,8,46,47,48,49,52,53,54,55,56,57,58
5	12,13,14,34	9,10,11,12,21,22,23,24,25,26

$$\begin{cases} V_i = rand \\ D_i = rand \\ A_i = lb_i + rand(ub_i - lb_i) \end{cases} \quad (24)$$

where O_i is the candidate solution, lb_i and ub_i represent the lower and upper bounds of the search space, and $rand$ is a random number between 0 and 1. The next step involves updating the densities and volumes of each candidate solution for the next iteration, calculated using Equations 25, 26 respectively.

$$D_i^{t+1} = D_i^t + rand(D_{best} - D_i^t) \quad (25)$$

$$V_i^{t+1} = V_i^t + rand(V_{best} - V_i^t) \quad (26)$$

Where D_i^t and V_i^t are the density and volume of the i^{th} solution at iteration t , D_{best} and V_{best} are the density and volume of the best solution found so far. The transfer operator (TF) and density factor (d) are then used to shift from exploration to exploitation, computed using Equations 27, 28 respectively.

configuration is identified. The initial positions for the population are calculated using Equation 23.

$$O_i = lb_i + rand(ub_i - lb_i); \quad i = 1, 2, 3, \dots, N \quad (23)$$

The Archimedes variables namely volume (V), density (D), and acceleration (A) for each solution are initialized using Equation 24.

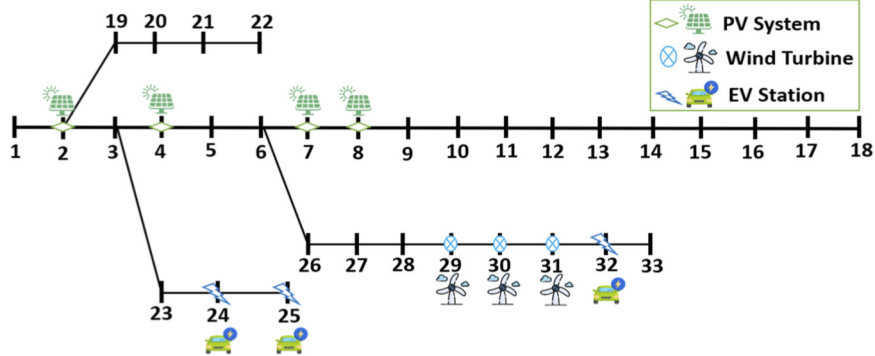


FIGURE 2 Integration of renewable energy sources and EVs in the IEEE 33-Bus system.

TABLE 3 Parameters of wind turbines, PV, and EVs in the IEEE 33-bus system.

System	Node	Wind speed (m/s)	Solar irradiation (w/m ²)	Power	
				Active (kw)	Reactive (kVAR)
Wind power generation	29	9		200	[-136.60, 151.11]
	30	11		266	[-92.13, 121.48]
	31	13		300	[-69.90, 106.67]
PV	2		600	12	[-21.90, 21.90]
	4		700	14	[-20.70, 20.70]
	7		800	16	[-19.18, 19.18]
	8		900	18	[-17.31, 17.31]
EVs (power station)	24			170.31	[-209.33, 209.33]
	25			156.74	[-211.43, 211.43]
	32			177.85	[-210.56, 210.56]

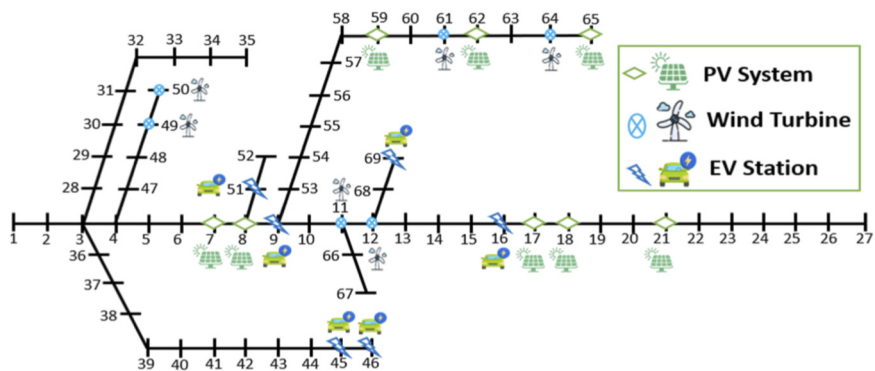


FIGURE 3 Integration of renewable energy sources and EVs in the IEEE 69-Bus system.

$$TF = \exp(t - t_{max}/t_{max}) \tag{27}$$

$$d^{t+1} = \exp(t - t_{max}/t_{max}) - (t/t_{max}) \tag{28}$$

Where t is the current iteration and t_{max} is the maximum number of iterations. Acceleration updates are handled through collision detection with neighboring solutions, where (A_i^{t+1}) if

TABLE 4 Parameters of wind turbines, PV, and EVs in the IEEE 69-bus system.

System	Node	Wind speed (m/s)	Solar irradiation (w/m ²)	Power	
				Active (kw)	Reactive (kVAr)
Wind power generation	11	4		33.31	[-41.29, 37.51]
	12	6		100.00	[-33.85, 32.48]
	49	8		166.66	[-26.40, 27.67]
	50	10		233.00	[-19.05, 22.47]
	61	12		300.00	[-11.67, 17.44]
	64	14		299.99	[-11.65, 17.40]
PV	7		350	6	[-29.19, 29.19]
	8		400	9	[-28.70, 28.70]
	17		650	12	[-27.80, 27.80]
	18		700	15	[-25.60, 25.60]
	21		950	18	[-24.00, 24.00]
	59		1,000	21	[-21.10, 21.10]
	62		1,200	24	[-18.00, 18.00]
	65		1,350	27	[-13.11, 13.11]
EVs (power station)	9			20.31	[-21.90, 21.90]
	16			20.74	[-21.80, 21.80]
	45			22.85	[-19.81, 19.81]
	46			-19.97	[-22.30, 22.30]
	51			16.44	[-24.94, 24.94]
	69			21.80	[-20.56, 20.56]

there is a collision or ($A_{i,best}^{t+1}$) otherwise using Equations 29, 30 respectively.

$$A_i^{t+1} = D_{mr} + V_{mr} \times A_{mr} / (D_i^{t+1} \times V_i^{t+1}) \tag{29}$$

$$A_{i,best}^{t+1} = D_{best} + V_{best} \times A_{best} / (D_i^{t+1} \times V_i^{t+1}) \tag{30}$$

Where A_{mr} is the acceleration of the neighboring solution with which a collision occurs, and D_{mr} and V_{mr} are the density and volume of the neighboring solution. These updates help simulate the physical movement of objects in a fluid, where collisions and buoyancy affect their acceleration. The normalized acceleration is calculated using Equation 31.

$$A_{i,norm}^{t+1} = u \times (A_i^{t+1} - A_{min} / A_{max} - A_{min}) \tag{31}$$

Where u is the normalization factor, set to 0.9 and 0.1, respectively. Normalization ensures that the acceleration values are scaled consistently, facilitating more controlled updates to the candidate solutions. Positions are updated based on acceleration using Equation 32 followed by the update of position relative to the best position using Equation 33.

$$x_i^{t+1} = x_i^t + C_1 \times rand \times A_{i,norm}^{t+1} \times d(x_{rand} - x_i^t) \tag{32}$$

$$x_i^{t+1} = x_{best}^t + F \times C_2 \times rand \times A_{i,norm}^{t+1} \times d(T \times x_{rand} - x_i^t) \tag{33}$$

The function (F) can be defined using Equation 34.

$$F = \begin{cases} +1, P \leq 0.5 \\ -1, P < 0.5 \end{cases} \tag{34}$$

Where C_1 and C_2 are constants, T increases with time ($C_3 \times TF$), and F is a flag to change direction ($P = 2 \times rand - C_4$). These equations direct candidate solutions to explore or refine their positions in the search space. Evaluate each updated solution using objective functions, then select the best based on fitness values (x_{best} , D_{best} , V_{best} , and A_{best}). The AOA algorithm's limitations can be addressed through reverse learning and multiverse-directing for changed reaching and mutation, which offers effective solutions as RMLAA by (Nguy et al., 2022). Initialize the population size NP , dimensions D , maximum iterations T , constants C_1, C_2, C_3, C_4 , upper and lower boundaries (ub, lb). The Reverse Learning Strategy aims to enhance the diversity of solutions and avoid local optima by generating new solutions based on the reverse of the current solutions. For a solution $S = (x_1, x_2, \dots, x_i, \dots, x_D)$ in the search space, the reverse solution $S' = (x_1', x_2', \dots, x_i', \dots, x_D')$ is calculated as reverse position of the i th dimension using Equation 35.

$$x_i' = a_i + b_i - x_i \tag{35}$$

x_i is the current position of the i th dimension, while a_i and b_i are the lower and upper bounds, respectively. The reverse position

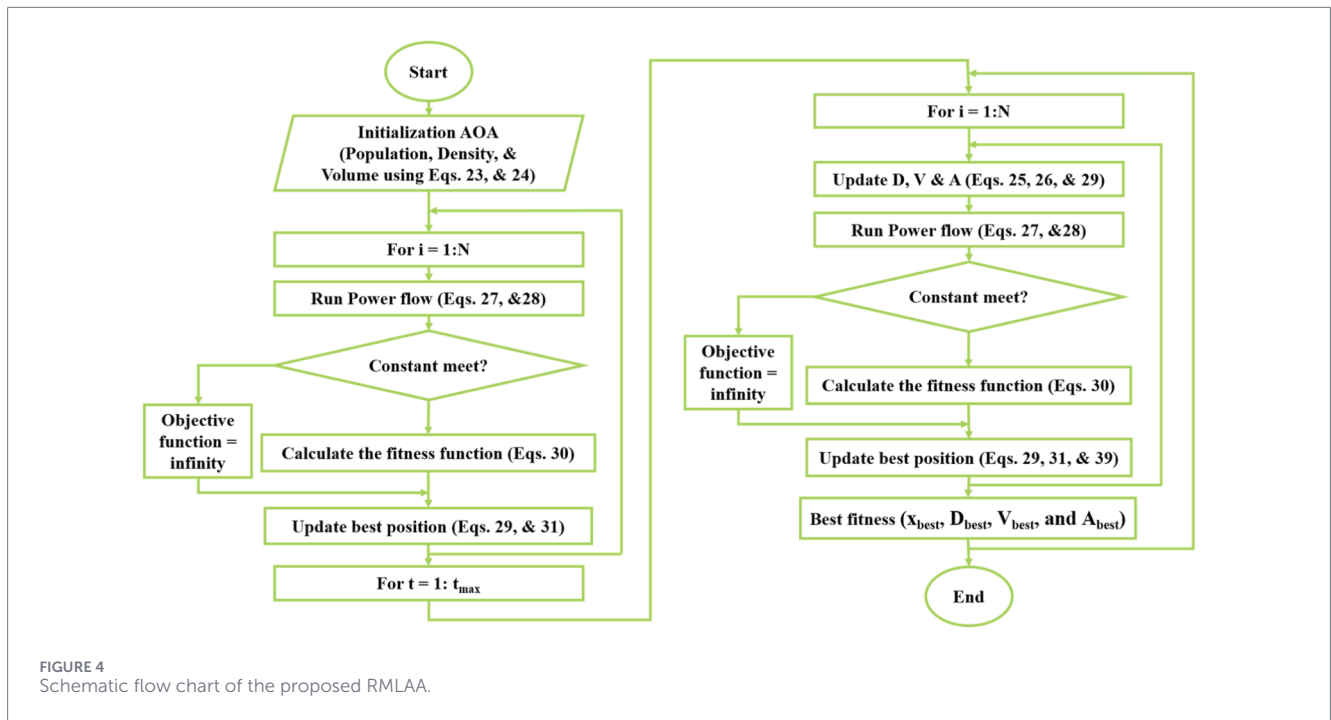


FIGURE 4 Schematic flow chart of the proposed RMLAA.

x'_i is computed to create a solution that is the mirror image of x_i within the defined bounds. The adjustment coefficient α_r is calculated using Equation 36 to control the influence of the reverse solution.

$$\alpha_r = R_{istar} \cdot \frac{rand(\beta, \gamma)}{D} \quad (36)$$

R_{istar} represents the distance between the ideal solution and the closest solution to the optimum, and $rand(\beta, \gamma)$ is a random value between β and γ . The new solution set S'_{new} is generated by combining the original solution S with the reverse solution using Equation 37.

$$S'_{new} = S + \alpha_r \quad (37)$$

The Multiverse-Directing Strategy boosts exploration by introducing varied search directions (F_{new}), with Equation 38 updating the RMLAA position.

$$F_{new} = \begin{cases} +1 \times rand & \text{if } P \leq 0.5 \\ -1 \times rand & \text{otherwise} \end{cases} \quad (38)$$

The updated position based on the Multiverse-Directing Strategy is given by Equation 39.

$$x_i^{t+1} = \begin{cases} x_i^t + \alpha_r \times C_1 \times rand \times A_{i,norm}^{t+1} \times d(x_{rand} - x_i^t), & \text{if } TF \leq 0.5 \\ x_{best}^t + F \times C_2 \times rand \times A_{i,norm}^{t+1} \times d(T \times x_{rand} - x_i^t), & \text{otherwise} \end{cases} \quad (39)$$

Where $rand$ is a random value between 0 and 1, and P is a probability value calculated as $P = 2 \times rand - C4$. Here, $C4$ is a constant that helps determine the threshold for altering the direction. In Figures 4, 5, the RMLAA process starts with randomly initializing candidate solutions and evaluating their fitness. The algorithm

iterates, selecting parents based on fitness, applying crossover and mutation, and keeping elite solutions. Weaker solutions are replaced, and local search operators refine the results. This continues until the termination condition is met, yielding an approximate optimal solution.

The study evaluates the proposed RMLAA algorithm's performance using the CEC17 benchmark test suite (Wu et al., 2017), which consists of 30 test functions of varying complexity, including unimodal ($f1-f3$), multimodal ($f4-f10$), hybrid ($f11-f20$), and compound ($f21-f29$) functions. Table 5, outlines the parameter settings for each algorithm. The optimization goal is to minimize the general objective function using Equation 40.

$$f(x) = \sum_{i=1}^D f_i(x) \quad (40)$$

Where $f_i(x)$ represents individual benchmark functions, x is the decision variable, and D is the dimension of the problem. Performance is measured by the mean objective value, which indicates the algorithm's average ability to find optimal solutions, and the standard deviation, which reflects the consistency of results across trials. Where T refers to the number of trials and $f(x_i)$ is the function value in the i th trial. The mean and standard deviation of the function value across trials can be calculated using Equations 41, 42 respectively.

$$Mean(f(x)) = \frac{1}{T} \sum_{i=1}^T f(x_i) \quad (41)$$

$$Std(f(x)) = \sqrt{\frac{1}{T} \sum_{i=1}^T (f(x_i) - Mean(f(x)))^2} \quad (42)$$

Figure 6 illustrates RMLAA's advantage in both convergence speed and stability, reaching an optimal solution within the first

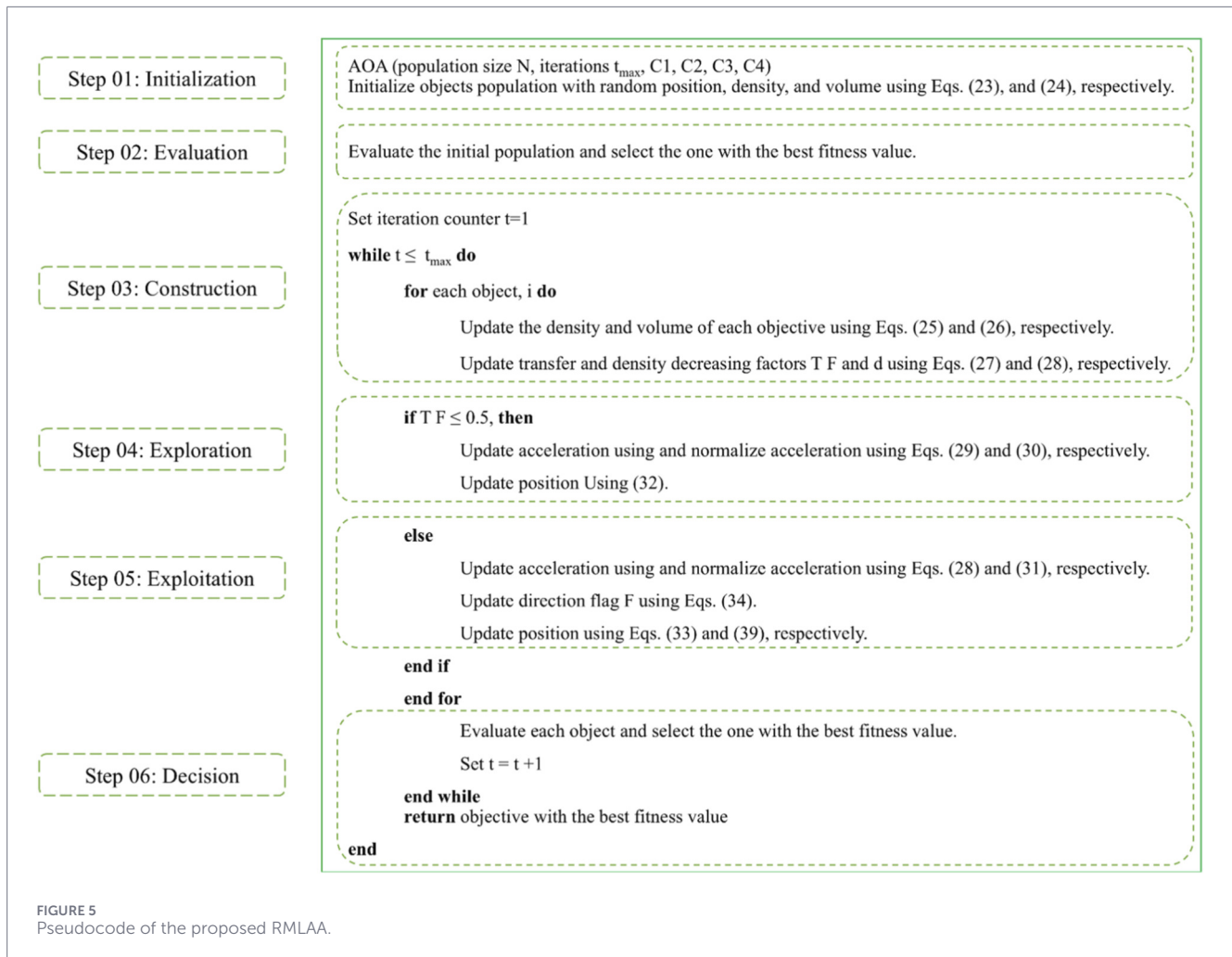


TABLE 5 Parameter settings for different algorithms.

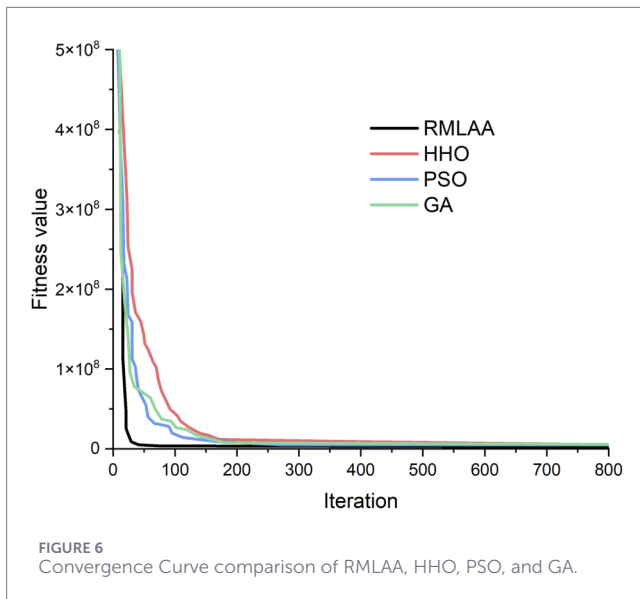
Algorithm	Parameter settings
RMLAA	Objective number = 30, $C_1 = 2, C_2 = 6, C_3 = 2, C_4 = 0.5$
AOA	Objective number = 30, $C_1 = 2, C_2 = 6, C_3 = 2, C_4 = 0.5$
GA	Population size = 30, Mutation Rate = 0.1, Crossover Rate = 0.9
PSO	Swarm size = 30, Maximum Velocity = 10, Minimum Velocity = -10, Inertia Weight = 0.9 to 0.4, Acceleration Coefficient = 1.49455
HHO	Hawk number = 30, Variable Changes Bounds = [-1,1]

100 iterations while maintaining a lower fitness value throughout. The other algorithms, while eventually converging, do so more slowly, requiring more iterations to achieve similar optimization results, making RMLAA more efficient. Table 6, compares the strategies influenced by the RMLAA's implementation with the original AOA algorithm, highlighting that while RMLAA achieves better convergence results than AOA in 20 out of 30 benchmark

functions, including $f_1, f_2, f_5, f_6, f_9-f_{14}, f_{16}-f_{19}, f_{21}-f_{24}, f_{27}, f_{28}$, it has a slightly longer execution time, as indicated by the average and runtime from thirty test runs for Reverse Learning, Multiverse-Directing, AOA, and RMLAA. Table 7, further demonstrates that the RMLAA consistently outperforms the GA, PSO, and HHO in terms of mean objective value and standard deviation, proving its superior accuracy and reliability. RMLAA shows better performance on functions $f_1, f_2, f_4, f_6, f_7, f_9-f_{11}, f_{13}-f_{15}, f_{17}-f_{21}$, and $f_{24}-f_{30}$, converging faster and delivering more reliable results overall. Figures 7A,B, illustrate the impact of varying wind speeds and solar irradiation on the optimization results obtained using the RMLAA.

4 Result analysis

The study uses RMLAA with a 30-population size and 70 iterations to optimize switch states and reactive power of new energy sources and EVs. The optimization dimensions are 15 for IEEE 33-bus and 25 for IEEE 69-bus systems. The Gauss-Seidel method, known for its simplicity and efficiency, is used for load flow calculations, making it ideal for hourly DNR operations in radial distribution networks.



4.1 Analysis of DNR solutions in different system

The RMLAA outperforms other methods in both the IEEE 33-bus and 69-bus systems, optimizing reactive power while significantly reducing power loss and improving voltage profiles. Its scalability ensures effective performance across different network sizes and complexities.

4.1.1 Convergent curve

Figure 8 shows that RMLAA outperforms GA, HHO, and PSO in the IEEE 33-bus and 69-bus systems. RMLAA achieves lower fitness values with fewer iterations, indicating faster convergence. In the 33-bus system, Figure 8A, RMLAA stabilizes by the 14th iteration, while others take longer. Similarly, in the 69-bus system, Figure 8B, RMLAA minimizes the fitness value by the 18th iteration, making it more effective in reducing power losses and improving voltage profiles.

4.1.2 DNR analysis

Tables 8, 9 show that RMLAA consistently outperforms GA, HHO, and PSO in optimizing tie-switch configurations for the IEEE 33-bus and 69-bus systems. As shown in Figure 9, in the IEEE 33-bus system, RMLAA reconfigured switches to 7, 9, 28, 16, and 13 in 5.93 s, significantly faster than GA (8.76 s), HHO (15.38 s), and PSO (9.08 s). For the IEEE 69-bus system, RMLAA reconfigured to 56, 61, 18, 42, and 13 in 6.96 s, outperforming GA (14.53 s), HHO (16.27 s), and PSO (11.38 s). This demonstrates RMLAA's superior speed and efficiency in solving DNR problems.

4.1.3 Power loss analysis

For the IEEE 33-bus system, as shown in Table 10, RMLAA reduced active power losses from 210.79 kW to 62.48 kW, a 70.35%

reduction, and reactive power losses from 113.42 kVAr to 59.37 kVAr, a 47.65% improvement. In comparison, GA, HHO, and PSO achieved active power loss reductions of 28.17%, 50.78%, and 30.58%, respectively, and reactive power loss reductions of 13.93%, 6.68%, and 3.39%. Figure 10a highlights the significant reduction decrease in branches like Branch 9 (from 39.2 kW to 11.3 kW) and Branch 4 (from 35 kW to 3.5 kW) after DNR. For the IEEE 69-bus system, Table 11, shows that RMLAA reduced active power losses by 69.08%, from 231.38 kW to 71.52 kW, and reactive power losses by 26.01%, from 107.25 kVAr to 79.36 kVAr. GA, HHO, and PSO achieved active power loss reductions of 57.97%, 63.73%, and 53.40%, with reactive power loss reductions of 12.84%, 24.82%, and 10.22%, respectively. Figure 10b illustrates significant reductions, notably in Branch 56, where losses dropped from 33.7 kW to 2.9 kW after DNR. This result highlights the efficiency of the DNR system in significantly reducing active and reactive power losses.

4.1.4 Voltage profile improvement analysis

In the IEEE 33-bus system, as shown in Table 12, RMLAA reduced voltage deviation from 0.0893 pu to 0.0396 pu, with a maximum voltage of 0.9995 pu and a minimum of 0.9777 pu after DNR. In comparison, GA, HHO, and PSO achieved voltage deviations of 0.0621 pu, 0.0487 pu, and 0.0562 pu, respectively. Figures 11a, 12a demonstrate RMLAA's superior performance in maintaining stable voltage profiles and minimizing deviations across buses, particularly outperforming other methods. For the IEEE 69-bus system, Table 13, shows RMLAA reduced voltage deviation from 0.08584 pu to 0.04090 pu, with a maximum voltage of 0.9994 pu and a minimum of 0.9821 pu. GA, HHO, and PSO achieved deviations of 0.04702 pu, 0.04613 pu, and 0.04725 pu, respectively. Figures 11b, 12b further confirm RMLAA's effectiveness in improving voltage stability across the system. This result highlights the reliability of the DNR system in improving and stabilizing the voltage profile across the network.

4.1.5 Optimization of reactive power

In reactive power optimization, RMLAA shows improved performance over GA, HHO, and PSO by providing balanced outputs across critical nodes in both the 33-bus and 69-bus systems. In the 33-bus system, as shown in Table 14, RMLAA achieves -24.57 kVAr and -83.49 kVAr at wind Nodes 29 and 30, with stable values for PV and EV stations. Similarly, in the 69-bus system, as indicated in Table 15, RMLAA provides efficient reactive power control, such as 20.34 kVAr at wind Node 11 and balanced results at key PV and EV nodes, demonstrating stability and control across renewable and EV integrations.

4.2 Discussion and validation

The proposed RMLAA improves efficiency and reliability in DNR by reducing power losses and enhancing voltage stability. In the IEEE 33-bus system, it reduces active and reactive power losses by 70.35% and 47.65%, and in the IEEE 69-bus

TABLE 6 Comparison of AOA and RMLAA performance across functions.

Function (x)	Reverse learning		Multiverse-directing		AOA		RMLAA	
	Avg	Runtime (sec.)	Avg	Runtime (sec.)	Avg	Runtime (sec.)	Avg	Runtime (sec.)
<i>f1</i>	1.11E + 01	34.3	1.46E + 01	34.2	4.29E + 00	33.969	3.75E + 00	39.559
<i>f2</i>	1.11E + 01	34.12	1.54E + 01	34.02	3.15E + 00	33.799	2.89E + 00	35.469
<i>f3</i>	5.52E-02	47.23	5.58E-02	47.09	1.30E + 00	46.379	2.48E + 00	50.079
<i>f4</i>	4.59E + 02	46	1.45E + 01	45.86	1.34E + 00	45.199	2.15E + 00	49.699
<i>f5</i>	1.38E + 02	42	7.86E + 03	41.87	8.00E + 02	48.059	6.42E + 00	48.209
<i>f6</i>	6.21E-02	89	2.11E-01	88.73	5.68E + 01	86.479	2.02E + 01	90.989
<i>f7</i>	2.44E-01	212	1.07E-01	211.36	3.25E + 00	204.559	1.36E + 01	209.119
<i>f8</i>	1.97E + 00	122	6.61E-01	121.63	7.36E + 00	118.159	8.21E + 00	118.049
<i>f9</i>	4.25E + 00	135	4.81E + 00	134.6	8.24E + 00	130.639	5.40E + 00	132.649
<i>f10</i>	1.01E + 01	234	2.03E + 01	233.3	1.20E + 04	225.679	2.11E + 02	230.819
<i>f11</i>	8.09E + 03	239	1.77E + 03	238.28	4.45E + 04	225.679	1.06E + 03	229.819
<i>f12</i>	8.09E + 01	239	3.65E + 01	238.28	1.67E + 02	230.479	2.39E + 01	233.439
<i>f13</i>	3.30E + 01	125	2.87E + 00	124.63	3.68E + 01	121.039	1.63E + 01	126.419
<i>f14</i>	1.09E + 01	100	1.62E + 00	100.7	3.06E + 01	97.999	1.36E + 01	100.459
<i>f15</i>	4.74E + 01	231	8.85E + 01	230.31	2.15E + 01	222.799	7.37E + 01	230.449
<i>f16</i>	2.59E + 01	132	1.88E + 01	131.6	4.83E + 01	127.759	1.40E + 01	129.279
<i>f17</i>	5.53E + 02	233	5.63E + 02	232.3	4.05E + 02	224.719	8.00E + 01	232.699
<i>f18</i>	1.46E + 01	105	3.70E + 01	104.69	2.50E + 02	105.679	2.00E + 02	108.959
<i>f19</i>	3.79E + 01	215	3.24E-01	214.36	4.16E + 01	207.439	3.96E + 01	211.489
<i>f20</i>	4.34E-02	310	4.11E-01	310.07	3.51E + 01	218.479	5.97E + 01	223.989
<i>f21</i>	8.92E + 02	234	2.03E + 01	339.92	6.61E + 01	328.399	2.20E + 01	333.979
<i>f22</i>	7.63E-01	326	6.22E + 01	325.02	1.00E + 02	313.999	6.89E + 01	317.139
<i>f23</i>	5.72E-02	316	7.63E-01	315.05	1.06E + 02	304.399	7.69E + 01	323.599
<i>f24</i>	4.75E + 01	294	6.63E + 01	293.12	7.48E + 01	283.279	4.22E + 01	291.199
<i>f25</i>	1.51E + 00	215	7.02E + 01	214.36	3.38E + 01	207.439	7.51E + 01	212.489
<i>f26</i>	2.78E + 02	264	8.03E + 01	263.21	2.73E + 01	232.879	6.45E + 01	239.039
<i>f27</i>	5.19E-01	264	7.74E + 01	263.21	8.38E + 01	254.479	7.51E + 01	257.509
<i>f28</i>	3.41E + 01	235	1.09E + 01	234.3	2.38E + 02	254.479	1.00E + 02	254.799
<i>f29</i>	3.14E + 01	230	8.37E + 01	230.31	3.25E + 01	222.799	4.99E + 01	230.449
<i>f30</i>	3.15E-01	186.47	6.88E + 01	185.91	1.52E + 02	187.759	4.31E + 02	190.509

Bold values indicate the best performance obtained among the compared methods.

system, by 69.08% and 26.01%. It also significantly improved voltage profiles, maintaining safe operational limits and grid stability. The algorithm effectively integrated Renewable Energy Sources (RES) and Electric Vehicles (EVs), such as PV systems and wind turbines, with optimized contributions in both bus systems. Additionally, compared to GA, PSO, and HHO, the RMLAA showed faster convergence, higher accuracy, and lower standard deviations, consistently meeting objectives of minimizing power losses and improving voltage profiles under dynamic conditions.

The proposed approach enhances the efficiency of the distribution network by substantially reducing active and reactive power losses, thereby minimizing energy waste and ensuring optimal power flow throughout the network. This improvement is achieved through the optimization of tie-switch configurations and the regulation of reactive power contributions from integrated Renewable Energy Sources (RES) and Electric Vehicles (EVs). For instance, in the IEEE 33-bus system, active power losses were reduced by 70.35%, from 210.79 kW to 62.48 kW, and reactive power losses decreased by 47.65%, from 113.42 kVAr to

TABLE 7 Comparison of Optimization Algorithms RMLAA vs. GA, PSO, and HHO.

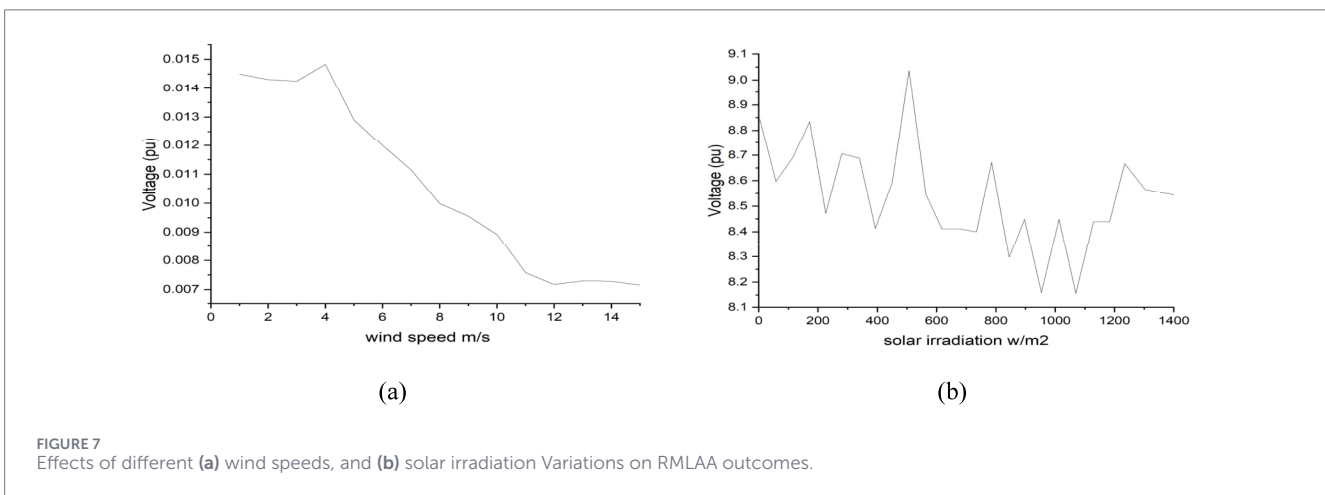
Function (x)	Measure	GA	PSO	HHO	RMLAA
f1	Mean	4.52E + 04	1.38E + 03	6.02E + 02	3.60E + 02
	Std. Dev.	8.57E + 02	6.59E + 02	1.48E + 03	7.23E + 03
f2	Mean	7.82E + 07	4.80E + 05	1.28E + 06	4.84E + 05
	Std. Dev.	3.64E + 07	3.26E + 06	4.90E + 06	1.48E + 06
f3	Mean	1.31E + 03	9.10E + 02	5.32E + 02	5.84E + 02
	Std. Dev.	3.66E + 02	6.61E + 02	5.94E + 02	7.17E + 02
f4	Mean	5.82E + 01	3.92E + 01	3.78E + 01	2.70E + 01
	Std. Dev.	2.89E + 01	4.84E + 01	4.03E + 01	4.01E + 01
f5	Mean	9.84E + 00	1.26E + 01	1.61E + 01	1.18E + 01
	Std. Dev.	7.83E + 00	1.18E + 01	1.15E + 01	1.11E + 01
f6	Mean	8.47E + 02	6.57E + 02	5.43E + 02	5.21E + 02
	Std. Dev.	2.32E + 02	5.61E + 02	6.14E + 02	6.01E + 02
f7	Mean	7.67E + 03	6.12E + 03	5.98E + 03	4.74E + 03
	Std. Dev.	1.84E + 03	4.90E + 03	5.84E + 03	5.65E + 03
f8	Mean	2.71E + 04	1.84E + 04	1.34E + 04	1.58E + 04
	Std. Dev.	9.84E + 03	1.75E + 04	1.94E + 04	9.71E + 03
f9	Mean	4.95E + 02	3.87E + 02	3.69E + 02	3.21E + 02
	Std. Dev.	1.78E + 02	4.01E + 02	3.52E + 02	3.48E + 02
f10	Mean	9.62E + 01	7.34E + 01	6.49E + 01	7.14E + 01
	Std. Dev.	4.28E + 01	6.15E + 01	5.83E + 01	5.99E + 01
f11	Mean	8.46E + 03	6.92E + 03	5.97E + 03	5.74E + 03
	Std. Dev.	4.34E + 03	4.61E + 03	5.12E + 03	4.09E + 03
f12	Mean	2.34E + 04	1.37E + 04	1.47E + 04	1.58E + 04
	Std. Dev.	9.01E + 03	8.21E + 03	7.56E + 03	7.30E + 03
f13	Mean	5.67E + 02	4.34E + 02	3.92E + 02	3.20E + 02
	Std. Dev.	3.14E + 02	3.21E + 02	3.12E + 02	3.10E + 02
f14	Mean	1.31E + 01	1.03E + 01	1.09E + 01	9.94E + 00
	Std. Dev.	6.24E + 00	5.64E + 00	5.43E + 00	5.29E + 00
f15	Mean	8.74E + 02	6.84E + 02	5.74E + 02	5.43E + 02
	Std. Dev.	3.67E + 02	3.89E + 02	3.43E + 02	3.31E + 02
f16	Mean	2.48E + 04	1.52E + 04	1.57E + 04	1.63E + 04
	Std. Dev.	7.89E + 03	8.21E + 03	7.78E + 03	7.61E + 03
f17	Mean	6.94E + 03	5.32E + 03	4.78E + 03	4.14E + 03
	Std. Dev.	3.43E + 03	4.21E + 03	3.99E + 03	3.31E + 03
f18	Mean	4.21E + 03	3.28E + 03	3.74E + 03	3.14E + 03
	Std. Dev.	2.79E + 03	2.34E + 03	2.32E + 03	2.31E + 03
f19	Mean	9.84E + 02	7.43E + 02	6.21E + 02	6.13E + 02
	Std. Dev.	3.31E + 02	4.21E + 02	3.87E + 02	3.90E + 02
f20	Mean	7.18E + 01	5.62E + 01	4.98E + 01	4.52E + 01
	Std. Dev.	3.43E + 01	3.31E + 01	3.21E + 01	3.16E + 01

(Continued)

TABLE 7 Continued

Function (x)	Measure	GA	PSO	HHO	RMLAA
f21	Mean	3.84E + 01	2.84E + 01	2.43E + 01	2.33E + 01
	Std. Dev.	1.98E + 01	1.78E + 01	1.61E + 01	1.57E + 01
f22	Mean	4.27E + 01	4.92E + 01	4.32E + 01	4.86E + 01
	Std. Dev.	2.84E + 01	2.43E + 01	2.31E + 01	2.28E + 01
f23	Mean	8.74E + 02	6.92E + 02	5.83E + 02	6.74E + 02
	Std. Dev.	4.21E + 02	4.01E + 02	3.87E + 02	3.71E + 02
f24	Mean	2.12E + 03	1.67E + 03	1.48E + 03	1.43E + 03
	Std. Dev.	7.31E + 02	5.21E + 02	5.89E + 02	6.17E + 02
f25	Mean	3.84E + 02	2.94E + 02	2.61E + 02	2.52E + 02
	Std. Dev.	1.76E + 02	1.48E + 02	1.31E + 02	1.12E + 02
f26	Mean	1.29E + 04	1.31E + 04	1.11E + 04	1.04E + 04
	Std. Dev.	8.43E + 03	7.62E + 03	7.28E + 03	7.04E + 03
f27	Mean	5.23E + 03	3.96E + 03	3.21E + 03	3.02E + 03
	Std. Dev.	2.34E + 03	1.87E + 03	1.74E + 03	1.49E + 03
f28	Mean	7.89E + 02	6.14E + 02	5.32E + 02	6.08E + 02
	Std. Dev.	3.12E + 02	2.76E + 02	2.58E + 02	2.54E + 02
f29	Mean	1.56E + 04	1.21E + 04	9.84E + 03	1.18E + 04
	Std. Dev.	5.21E + 03	5.74E + 03	5.32E + 03	5.67E + 03
f30	Mean	3.48E + 03	2.74E + 03	2.31E + 03	2.23E + 03
	Std. Dev.	1.57E + 03	1.43E + 03	1.32E + 03	1.28E + 03

Bold values indicate the best performance obtained among the compared methods.



59.37 kVAR. Similarly, in the IEEE 69-bus system, active power losses were reduced by 69.08%, from 231.38 kW to 71.52 kW, and reactive power losses by 26.01%, from 107.25 kVAR to 79.36 kVAR.

Reliability is further demonstrated through significant improvements in voltage stability, ensuring consistent voltage

profiles under varying load and generation conditions. For the IEEE 33-bus system, voltage deviation was reduced from 0.0893 pu to 0.0396 pu, with a maximum voltage of 0.9995 pu and a minimum of 0.9777 pu. In the IEEE 69-bus system, voltage deviation was reduced from 0.08584 pu to 0.04090 pu, with a maximum voltage of 0.9994 pu and a minimum of 0.9821 pu. These improvements

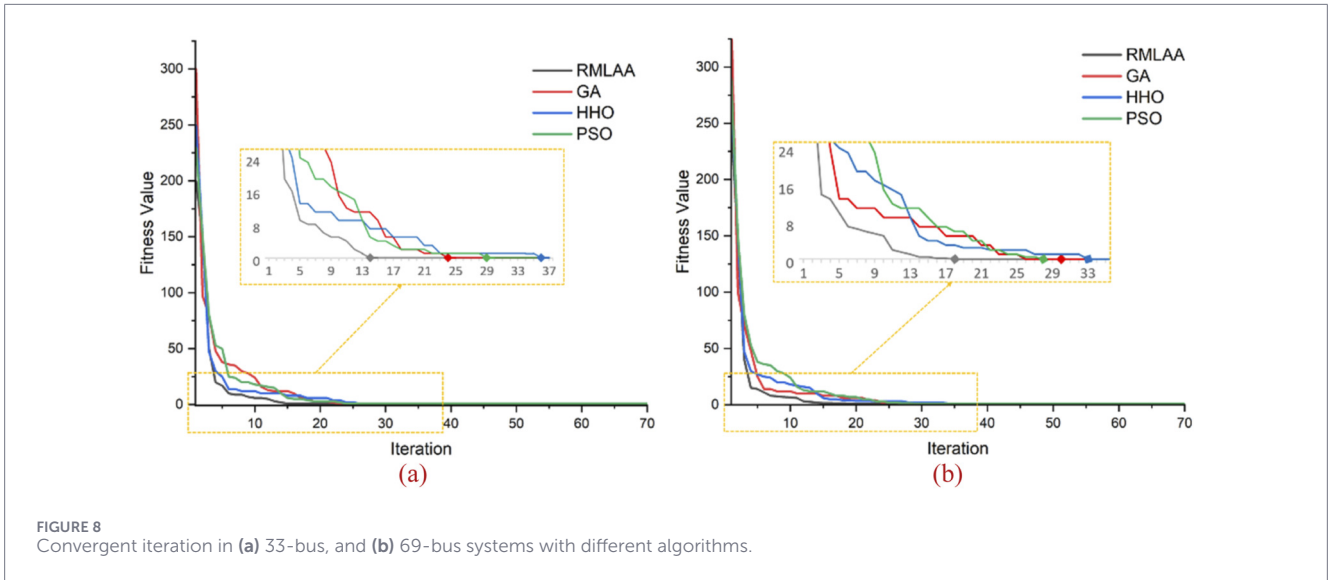


FIGURE 8 Convergence iteration in (a) 33-bus, and (b) 69-bus systems with different algorithms.

TABLE 8 Optimal tie-switches in IEEE 33-bus system.

Algorithms	Before DNR	After DNR	Time (sec.)
RMLAA	33-34-35-36-37	7-9-28-16-13	5.93
GA	33-34-35-36-37	7-9-37-32-13	8.76
HHO	33-34-35-36-37	7-11-27-37-13	15.38
PSO	33-34-35-36-37	7-10-37-32-14	9.08

TABLE 9 Optimal tie-switches in IEEE 69-bus system.

Algorithms	Before DNR	After DNR	Time (sec.)
RMLAA	69-70-71-72-73	56-61-18-42-13	6.96
GA	69-70-71-72-73	58-63-18-71-10	14.53
HHO	69-70-71-72-73	56-61-19-10-13	16.27
PSO	69-70-71-72-73	57-63-18-71-10	11.38

in stabilizing the voltage profile were achieved despite fluctuations caused by photovoltaic (PV) and wind irradiation, demonstrating the system’s robustness and adaptability to the variability of RES and EVs.

The efficacy of the proposed approach was validated through rigorous testing on IEEE 33-bus and 69-bus systems, as well as the CEC17 benchmark suite. It was consistently compared against various algorithms, including GA, PSO, and HHO. The results demonstrated that the proposed method surpassed these algorithms in terms of reducing power losses, stabilizing voltage profiles, and achieving greater computational efficiency. Specifically, the proposed method reduced computation time by up to 61.5% for the IEEE 33-bus system and by 57.2% for the IEEE 69-bus system in comparison to HHO.

4.3 Comparative study

This section presents a comparative analysis of the DNR approaches applied to the IEEE 33-bus and 69-bus systems, highlighting a detailed comparison of various models based on open switch configurations, power losses after reconfiguration, and computational time.

4.3.1 Comparative analysis of 33-bus test system

Table 16, compares various algorithms applied to the IEEE 33-bus system, highlighting power losses and computation times after reconfiguration. The proposed RMLAA achieved the best results, with the lowest power loss of 62.48 kW in just 5.93 s, reconfiguring switches to 7, 9, 28, 16, and 13. In contrast, MILP and NCUP both recorded power losses of 139.55 kW with computation times of 47.03 and 52.8 s, respectively, while MIQCP achieved a lower loss of 122.8 kW in 30.2 s. HBMO also resulted in losses of 139.55 kW but took 32.7 s. MPGSA achieved a notable improvement with 72.23 kW in 7.2 s. Among ant-based algorithms, AACOA and HC-ACO had losses of 136.8 kW and 139.8 kW, with HC-ACO completing in 6.852 s. DTLBO and MCCUM reported losses of 119.5 kW and 139.5 kW, respectively. RMLAA outperformed all methods in both power loss reduction and speed, proving the most efficient for DNR.

4.3.2 Comparative analysis of 69-bus test system

Table 17, compares optimization algorithms for the IEEE 69-bus system, focusing on power losses and computation times after reconfiguration. The proposed RMLAA achieved the lowest power loss of 71.52 kW in 6.96 s with a switch configuration of 56, 61, 18, 42, 13, significantly outperforming other methods. In comparison, RGA and NCUP recorded higher power losses of 94.94 kW and 98.6 kW, with computation times of 23.63 and 15.3 s, respectively. MTS achieved slightly better results with

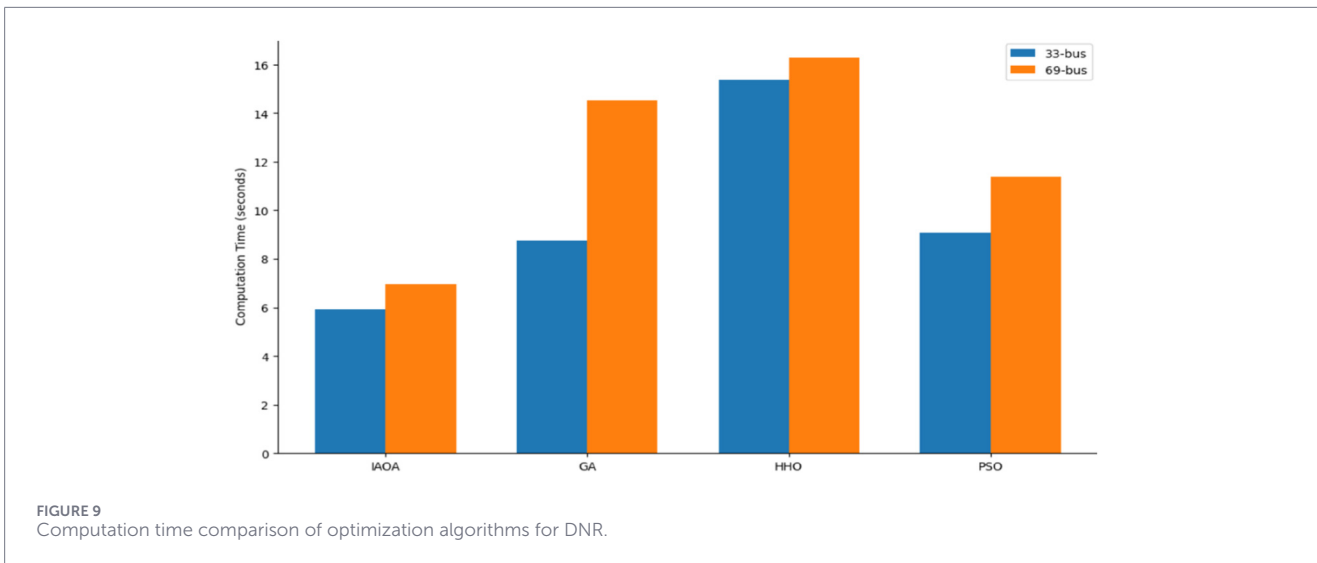


TABLE 10 Loss generation during transmission in 33-bus system.

Algorithm	Active (Ploss-KW)		Active power loss reduction (%)	Reactive (Qloss-kVAr)		Reactive power loss reduction (%)
	Before DNR	After DNR		Before DNR	After DNR	
RMLAA	210.79	62.48	70.35	113.42	59.37	47.65
GA	210.79	151.39	28.17	113.42	97.62	13.93
HHO	210.79	103.74	50.78	113.42	105.84	6.68
PSO	210.79	146.31	30.58	113.42	109.57	3.39

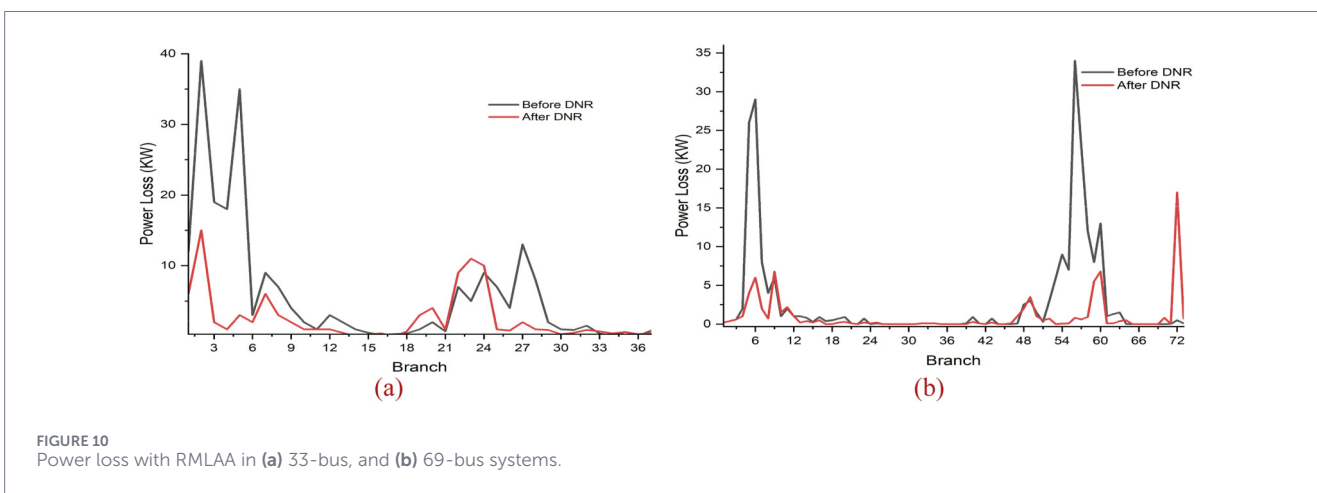


TABLE 11 Loss generation during transmission in 69-bus system.

Algorithm	Active (Ploss-KW)		Active power loss reduction (%)	Reactive (Qloss-kVAr)		Reactive power loss reduction (%)
	Before DNR	After DNR		Before DNR	After DNR	
RMLAA	231.38	71.52	69.08	107.25	79.36	26.01
GA	231.38	97.23	57.97	107.25	93.47	12.84
HHO	231.38	83.92	63.73	107.25	80.62	24.82
PSO	231.38	107.82	53.40	107.25	96.28	10.22

TABLE 12 Voltage variations after DNR in the IEEE 33-bus system.

Algorithm	Voltage deviation (pu)		Voltage (pu)	
	Before DNR	After DNR	Maximum	Minimum
RMLAA	0.0893	0.0396	0.9995	0.9777
GA	0.0893	0.0621	0.9995	0.9645
HHO	0.0893	0.0487	0.9995	0.9642
PSO	0.0893	0.0562	0.9995	0.9662

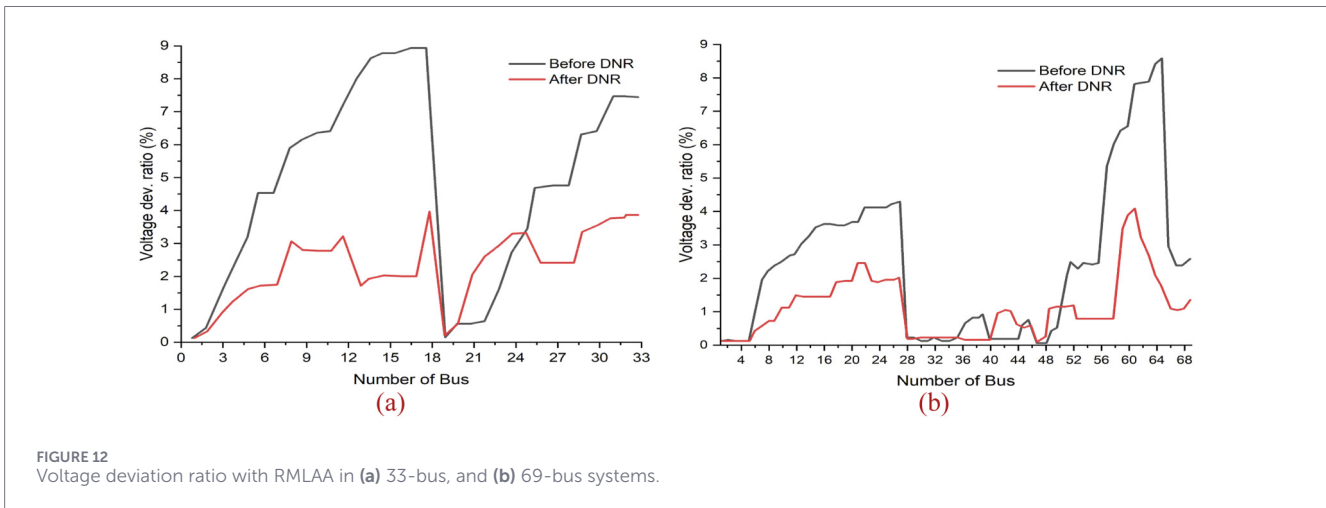
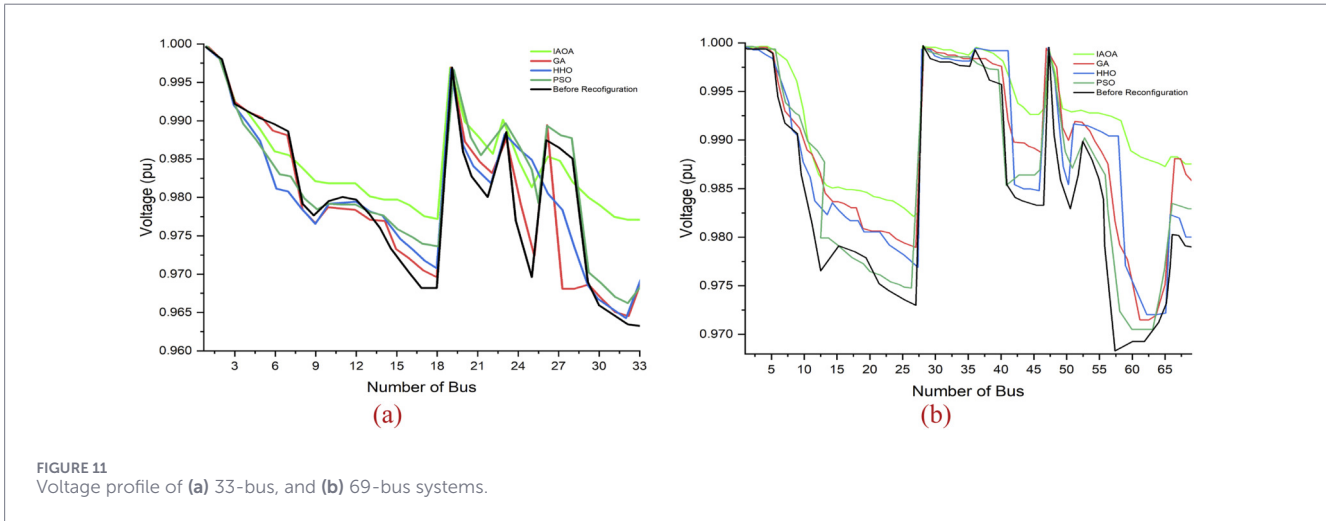


TABLE 13 Voltage variations after DNR in the IEEE 69-bus system.

Algorithm	Voltage deviation (pu)		Voltage (pu)	
	Before DNR	After DNR	Maximum	Minimum
RMLAA	0.08584	0.04090	0.9994	0.9821
GA	0.08584	0.04702	0.9994	0.9714
HHO	0.08584	0.04613	0.9994	0.9720
PSO	0.08584	0.04725	0.9994	0.9705

TABLE 14 Reactive power output of 33-bus system.

System	Node	Reactive power (kVAr)			
		RMLAA	GA	HHO	PSO
Wind power generation	29	-24.57	84.97	-129.37	84.24
	30	-83.49	79.56	79.54	80.03
	31	5.37	-30.04	78.98	-9.74
PV	2	22.18	-14.13	-20.11	8.96
	4	19.94	-17.86	14.64	-20.39
	7	-18.76	16.58	14.28	09.98
	8	4.95	-5.36	14.57	-6.17
EVs (power station)	24	57.48	189.74	129.96	20.08
	25	-52.83	30.16	-119.73	-170.53
	32	109.61	200.05	107.16	201.13

TABLE 15 Reactive power output of 69-bus system.

System	Node	Reactive power (kVAr)			
		RMLAA	GA	HHO	PSO
Wind power generation	11	20.34	20.29	-11.83	23.07
	12	18.26	24.87	-26.39	-2.36
	49	4.97	4.83	-7.62	4.52
	50	19.53	19.52	-14.03	18.73
	61	5.84	7.06	-0.11	5.76
	64	-5.15	9.96	3.67	-11.48
PV	7	39.28	31.47	30.04	1.94
	8	15.03	15.02	25.23	14.16
	17	28.16	28.27	20.47	28.30
	18	4.58	-7.92	10.07	20.07
	21	-4.46	3.98	2.02	-1.69
	59	13.74	11.63	9.76	11.95
	62	5.39	16.47	14.82	-3.57
	65	-10.08	-13.28	11.87	-12.06
EVs (power station)	9	-12.32	-10.94	4.17	-8.23
	16	-14.86	-6.43	1.36	-7.52
	45	4.06	4.06	14.29	3.18
	46	1.02	1.03	-4.73	-6.08
	51	-13.96	-11.27	20.05	-9.92
	69	-19.95	-2.04	19.47	-9.13

84.43 kW in 22.17 s. AACOA and MCCUM delivered losses of 89.24 kW and 92.1 kW, but their computation times were not reported. Similarly, DTLBO resulted in a loss of 90.76 kW without a specified time. Evolutionary algorithms like FGA and BGA produced 96.5 kW and 99.62 kW power losses, with

computation times of 20.47 and 10.3 s, respectively. FNSGA showed comparable performance with 87.83 kW, RMLAA proved superior, delivering the best balance between low power loss and fast computation time.

5 Conclusion

This research introduces an advanced distribution network reconfiguration model that incorporates renewable energy sources such as wind and photovoltaic systems, in addition to electric vehicles. The proposed model employs multi-objective optimization techniques to minimise both active and reactive power losses, mitigate voltage deviations, and enhance overall network performance. The model's effectiveness was verified using the IEEE 33-bus and 69-bus test systems, where it achieved significant improvements in operational efficiency and reliability. The key findings of this research are as follows:

- In the IEEE 33-bus system, the RMLAA reduced active power losses by 70.35% (from 210.79 kW to 62.48 kW) and reactive power losses by 47.65% (from 113.42 kVAr to 59.37 kVAr). Similarly, in the IEEE 69-bus system, active power losses were reduced by 69.08% (from 231.38 kW to 71.52 kW) and reactive power losses by 26.01% (from 107.25 kVAr to 79.36 kVAr).
- The RMLAA improved voltage deviation in the IEEE 33-bus system from 0.0893 pu to 0.0396 pu, and in the IEEE 69-bus system, it enhanced voltage deviation from 0.08584 pu to 0.04090 pu.
- The RMLAA outperformed GA, HHO, and PSO in reducing power losses and improving voltage stability. Moreover, the RMLAA demonstrated superior computational efficiency, solving the IEEE 33-bus system in 5.93 s and the IEEE 69-bus system in 6.96 s.
- By leveraging reverse learning and a multiverse-directing mechanism, the RMLAA effectively balanced exploration and exploitation, achieving faster convergence and generating multiple optimal solutions. Performance on the CEC17 benchmark functions further validated its robustness and capability in navigating complex multi-objective optimization problems.
- The RMLAA consistently outperformed other algorithms, including heuristic and metaheuristic approaches such as NCUP, MILP, AACOA, and DTLBO, in terms of power loss reduction, voltage improvement, and computational efficiency. The RMLAA demonstrated superior performance across these metrics compared to both traditional and advanced optimization techniques.

Future research will focus on creating a hybrid optimization algorithm that merges RMLAA with other metaheuristics to improve convergence speed, accuracy, and adaptability for renewable energy and electric vehicles. Additional work will aim to scale the algorithm for larger networks, develop real-time applications, and integrate advanced energy storage systems to boost grid performance.

TABLE 16 Comparative analysis following Reconfiguration of the 33-bus test system.

Ref.	Model	Open switches	Power losses (kw)	Time (s)
Rao et al. (2011)	HSA	7,10,14,36,37	142.68	7.2
Taylor and Hover (2012)	QCP	7,9,14,32,37	139.50	14.3
	QP			41
Llorens-Iborra et al. (2012)	MILP	7,9,14,32,37	139.55	47.03
Ferdavani et al. (2013)	NCUP	7,9,14,32,37	139.55	52.8
Raju and Bijwe (2008)	BE	7,9,14,32,37	139.55	41
Ahmadi and Martí (2015a)	GT	7,9,14,32,37	139.60	46
Ahmadi and Martí (2015b)	MILP	7,9,14,32,37	139.55	15
	MIQCP			35.2
Ahmadi and Martí (2015c)	MIQP	7,9,14,32,25	122.8	30.2
Jasthi and Das (2018)	Heuristic	7,9,14,32,37	139.55	37
Esmaeilian and Fadaeinedjad (2015)	HSA	7,10,14,36,37	139.55	32.7
	HBMO			8
	ACO	7,9,14,32,37		64.4
Rajaram et al. (2015)	MPGSA	7,10,14,36,37	72.23	7.2
Saffar et al. (2011)	AACOA	7,10,14,32,37	136.80	—
Swarnkar et al. (2011)	AACO	7,9,14,32,37	139.55	30
Abdelaziz et al. (2012)	HC-ACO	7,9,14,32,37	139.80	6.852
Lotfipour and Afrakhte (2016)	DTLBO	7-9-14-28-32	115.7	—
Zin et al. (2012)	MCCUM	7-9-14-32-37	139.5	—
Taher and Karimi (2014)	BGA	7-9-14-32-37	139.5	—
Proposed method	RMLAA	7-9-28-16-13	62.48	5.93

TABLE 17 Comparative analysis after Reconfiguration for 69-bus test system.

Ref.	Model	Open switches	Power losses (kW)	Time (s)
Rao et al. (2011)	GA	14,53,61,69,70	103.29	—
	RGGA	13,17,55,61,69	100.28	—
Ferdavani et al. (2013)	Heuristic	11,14,21,56,62	106.67	—
	NCUP	13,58,61,69,70	99.72	—
Raju and Bijwe (2008)	BE	14,55,61,69,70	99.62	—
Abdelaziz et al. (2010)	MTS	14,55,61,69,70	99.40	15
Saffar et al. (2011)	AACOA	12,57,61,69,70	99.82	—
Lotfipour and Afrakhte (2016)	DTLBO	14,57,61,69,70	99.62	—
Sahoo and Prasad (2006)	FGA	12,20,58,64,69	113.8	50
	BGA			25
Zin et al. (2012)	MCCUM	70-71-15-56-62	99.62	—
Taher and Karimi (2014)	BGA	69-70-14-47-50	98.61	18
Eldurssi and O'Connell (2015)	FNSGA	14,57,61,69,70	99.62	20.2
Reddy and Reddy (2016)	DOA	14,57,61,69,70	99.62	7
Proposed method	RMLAA	56-61-18-42-13	71.52	6.96

Data availability statement

The data used in this research are incorporated within this article, further inquiries can be directed to the corresponding authors.

Author contributions

MT: Conceptualization, Data curation, Formal Analysis, Investigation, Methodology, Software, Writing – original draft. SA: Conceptualization, Data curation, Formal Analysis, Investigation, Methodology, Software, Supervision, Writing – original draft, Writing – review and editing. MM: Conceptualization, Data curation, Formal Analysis, Investigation, Methodology, Software, Supervision, Writing – review and editing. MH: Investigation, Methodology, Visualization, Writing – review and editing. TA: Methodology, Software, Writing – review and editing, Investigation, Validation. AH: Conceptualization, Formal Analysis, Investigation, Data curation, Validation, Visualization, Methodology, Software, Writing – review and editing. GS: Investigation, Methodology, Supervision, Writing – review and editing, Validation.

Funding

The author(s) declared that financial support was not received for this work and/or its publication.

References

- Abdelaziz, A. Y., Mohamed, F. M., Mekhamer, S. F., and Badr, M. A. L. (2010). Distribution system reconfiguration using a modified tabu search algorithm. *Electr. Power Syst. Res.* 80 (8), 943–953. doi:10.1016/j.epsr.2010.01.001
- Abdelaziz, A. Y., Osama, R. A., and El-Khodary, S. M. (2012). Reconfiguration of distribution systems for loss reduction using the hyper-cube ant colony optimisation algorithm. *IET Gener. Transm. Distrib.* 12 (2), 176–187. doi:10.1049/iet-gtd.2011.0281
- Abdelsattar, M., Ismeil, M. A., Aly, M. M., and Abu-Elwfa, S. S. (2024). Analysis of renewable energy sources and electrical vehicles integration into microgrid. *IEEE Access* 12, 66822–66832. doi:10.1109/access.2024.3399124
- Ahmadi, H., and Marti, J. R. (2015a). Mathematical representation of radiality constraint in distribution system reconfiguration problem. *Int. J. Electr. Power Energy Syst.* 64, 293–299. doi:10.1016/j.ijepes.2014.06.076
- Ahmadi, H., and Marti, J. R. (2015b). Linear current flow equations with application to distribution systems reconfiguration. *IEEE Trans. Power Syst.* 30 (4), 2073–2080. doi:10.1109/TPWRS.2014.2360363
- Ahmadi, H., and Marti, J. R. (2015c). Distribution system optimization based on a linear power-flow formulation. *IEEE Trans. Power Del.* 30 (1), 25–33. doi:10.1109/TPWRD.2014.2300854
- Alshareef, S. M., and Fathy, A. (2023). Efficient Red KITE optimization algorithm for integrating the renewable sources and electric vehicle fast charging stations in radial distribution networks. *Mathematics* 11 (15), 3305. doi:10.3390/math11153305
- Arulprakasam, S., and Muthusamy, S. (2021). Reconfiguration of distribution networks using rain-fall optimization with non-dominated sorting. *Appl. Soft Comput.* 115, 108200. doi:10.1016/j.asoc.2021.108200
- Cai, X. B., and Zhao, X. (2023). “Optimized operation of electric thermal multi-energy flow coupling system under the solar thermal power station and carbon trading mechanism,” in *Second international conference on energy, power, and electrical technology (ICEPET 2023)*. doi:10.12204/j.issn.1000-7229.2024.03.003
- Castro, F., Canizes, B., Soares, J., Almeida, J., and Vale, Z. (2024). Comprehensive framework for distribution network multi-investment expansion planning: emissions, uncertainty, and resource remuneration integration. *Energy Convers. Manag.* 316 (118734), 118734. doi:10.1016/j.enconman.2024.118734
- Duan, F., Basem, A., Jasim, D. J., Belhaj, S., Eslami, M., Khajehzadeh, M., et al. (2024). A new multi-objective-stochastic framework for reconfiguration and wind

Conflict of interest

The author(s) declared that this work was conducted in the absence of any commercial or financial relationships that could be construed as a potential conflict of interest.

Generative AI statement

The author(s) declared that generative AI was not used in the creation of this manuscript.

Any alternative text (alt text) provided alongside figures in this article has been generated by Frontiers with the support of artificial intelligence and reasonable efforts have been made to ensure accuracy, including review by the authors wherever possible. If you identify any issues, please contact us.

Publisher’s note

All claims expressed in this article are solely those of the authors and do not necessarily represent those of their affiliated organizations, or those of the publisher, the editors and the reviewers. Any product that may be evaluated in this article, or claim that may be made by its manufacturer, is not guaranteed or endorsed by the publisher.

energy resource allocation in distribution network incorporating improved dandelion optimizer and uncertainty. *Sci. Rep.* 14 (1), 20857. doi:10.1038/s41598-024-71672-0

Duong, M. P., Le, M.-H., Nguyen, T. T., Duong, M. Q., and Doan, A. T. (2025). Economic and technical aspects of power grids with electric vehicle charge stations, sustainable energies, and compensators. *Sustainability* 17 (1), 376. doi:10.3390/su17010376

Eldurssi, A. M., and O’Connell, R. M. (2015). A fast nondominated sorting guided genetic algorithm for multi-objective power distribution system Reconfiguration problem. *IEEE Trans. Power Syst.* 30 (2), 593–601. doi:10.1109/TPWRS.2014.2332953

Elymany, M. M., Enany, M. A., and Elsonbaty, N. A. (2024). Hybrid optimized-ANFIS based MPPT for hybrid microgrid using zebra optimization algorithm and artificial gorilla troops optimizer. *Energy Convers. Manag.* 299 (117809), 117809. doi:10.1016/j.enconman.2023.117809

Emimal, K. N., and Mahiban, L. N. (2023). Enhancing electric vehicle reliability and integration with renewable energy: a multi-faceted review. London: Qeios, 6, 1–9. doi:10.32388/G7VHLA.3

Esmailian, H. R., and Fadaeinedjad, R. (2015). Energy loss minimization in distribution systems utilizing an enhanced reconfiguration method integrating distributed generation. *IEEE Syst. J.* 9 (4), 1430–1439. doi:10.1109/JSYST.2014.2341579

Ferdavani, A. K., Zin, A. A. M., Khairuddin, A., and Naeni, M. M. (2013). Reconfiguration of distribution system through two minimum-current neighbour-chain updating methods. *IET Gener. Transm. Distrib.* 7 (12), 1492–1497. doi:10.1049/iet-gtd.2012.0737

Fose, N., Singh, A. R., Krishnamurthy, S., Ratshitanga, M., and Moodley, P. (2024). Empowering distribution system operators: a review of distributed energy resource forecasting techniques. *Heliyon* 10 (15), e34800. doi:10.1016/j.heliyon.2024.e34800

Gallego, L. A., Lopez-Lezama, J. M., and Carmona, O. G. (2022). A mixed-integer linear programming model for simultaneous optimal reconfiguration and optimal placement of capacitor banks in distribution networks. *IEEE Access* 10, 52655–52673. doi:10.1109/ACCESS.2022.3175189

Habib, H. U. R., Waqar, A., Farhan, B. S., Ahmad, T., Jahangiri, M., Ismail, M. M., et al. (2022). Analysis of optimal integration of EVs and DGs into CIGRE’s MV benchmark model. *IEEE Access* 10, 95949–95969. doi:10.1109/ACCESS.2022.3204311

Hashim, F. A., Hussain, K., Houssein, E. H., Mabrouk, M. S., and Al-Atabany, W. (2020). Archimedes optimization algorithm: a new metaheuristic algorithm for

- solving optimization problems. *Appl. Intell.* 51 (3), 1531–1551. doi:10.1007/s10489-020-01893-z
- Hijazi, H., and Thiébaux, S. (2015). Optimal distribution systems reconfiguration for radial and meshed grids. *Int. J. Electr. Power Energy Syst.* 72, 136–143. doi:10.1016/j.ijepes.2015.02.026
- Hizarci, H., Demirel, O., and Turkyay, B. E. (2022). Distribution network reconfiguration using time-varying acceleration coefficient assisted binary particle swarm optimization. *Eng. Sci. Technol. Int. J.* 35, 101230. doi:10.1016/j.jestch.2022.101230
- IRENA (2024). Irena.org. Available online at: https://www.irena.org/-/media/Files/IRENA/Agency/Publication/2024/Jul/Renewable_energy_highlights_FINAL_July_2024.pdf (Accessed: October 04, 2024).
- Jabr, R. A., Singh, R., and Pal, B. C. (2012). Minimum loss network reconfiguration using mixed-integer convex programming. *IEEE Trans. Power Syst.* 27 (2), 1106–1115. doi:10.1109/TPWRS.2011.2180406
- Jasthi, K., and Das, D. (2018). Simultaneous distribution system reconfiguration and DG sizing algorithm without load flow solution. *IET Gener. Transm. Distrib.* 12 (6), 1303–1313. doi:10.1049/iet-gtd.2017.0338
- Jiménez, A., Cabrera, P., Fernando Medina, J., Alberg Østergaard, P., and Lund, H. (2024). Smart energy system approach validated by electrical analysis for electric vehicle integration in islands. *Energy Convers. Manag.* 302 (118121), 118121. doi:10.1016/j.enconman.2024.118121
- Jin, W., Zhang, S., and Li, J. (2023). Robust planning of distributed generators in active distribution network considering network reconfiguration. *Appl. Sci.* 13 (13), 7747. doi:10.3390/app13137747
- Jo, S., Oh, J. Y., Lee, J., Oh, S., Moon, H. S., Zhang, C., et al. (2024). Hybrid genetic algorithm with k-nearest neighbors for radial distribution network reconfiguration. *IEEE Trans. Smart Grid* 15 (3), 2614–2624. doi:10.1109/TSG.2023.3324328
- Karimi, M., Oskuee, M. R. J., and Ravdanegh, S. N. (2019). An optimal solution for eco-reliability stochastic modeling of simultaneous reconfiguration of distribution networks and allocation of renewable energy resources, capacitors and d-facts. *Electr. & Electron. Eng.* 13 (4), 486–495. doi:10.2174/2352096512666190306142831
- Liemthong, R., Srithapon, C., Ghosh, P. K., and Chatthaworn, R. (2022). Home energy management strategy-based meta-heuristic optimization for electrical energy cost minimization considering TOU tariffs. *Energies* 15 (2), 537. doi:10.3390/en15020537
- Liu, S., and Gao, G. (2023). “Reactive power optimization strategy of distribution network based on second-order cone programming,” in *Sixth international conference on intelligent computing, communication, and devices (ICCD 2023)*. doi:10.1117/12.2682905
- Llorens-Iborra, F., Riquelme-Santos, J., and Romero-Ramos, E. (2012). Mixed-integer linear programming model for solving reconfiguration problems in large-scale distribution systems. *Electr. Power Syst. Res.* 88, 137–145. doi:10.1016/j.epsr.2012.01.014
- Lotfi, H. (2025). Stochastic bi-level modelling and optimization of dynamic distribution networks with DG and EV integration. *Energy Inf.* 8 (1), 98. doi:10.1186/s42162-025-00557-x
- Lotfi, H., Nikkhal, M. H., and Hajiabadi, M. E. (2025). Dynamic reconfiguration for energy management in EV and RES-based grids using IWOA. *World Electr. Veh. J.* 16 (8), 412. doi:10.3390/wevj16080412
- Lotfipour, A., and Afrakhte, H. (2016). A discrete teaching-learning-based optimization algorithm to solve distribution system reconfiguration in presence of distributed generation. *Int. J. Electr. Power Energy Syst.* 82, 264–273. doi:10.1016/j.ijepes.2016.03.009
- Mahmoud, A. M., Ezzat, M., Abdelaziz, A. Y., and Aleem, S. H. E. A. (2021). “A cost-benefit analysis of optimal active and reactive power compensators and voltage conditioners allocation in a real Egyptian distribution system,” in *2021 22nd international Middle East power systems conference (MEPCON)*. doi:10.1109/MEPCON50283.2021.9686207
- Mazumder, M., and Debbarma, S. (2020). EV charging stations with a provision of V2G and voltage support in a distribution network. *IEEE Syst. J.* 15 (1), 662–671. doi:10.1109/jsyst.2020.3002769
- Monteiro, R. V. A., Bonaldo, J. P., Da Silva, R. F., and Bretas, A. S. (2020). Electric distribution network reconfiguration optimized for PV distributed generation and energy storage. *Electr. Power Syst. Res.* 184, 106319. doi:10.1016/j.epsr.2020.106319
- Morsy, B., Hinneck, A., Pozo, D., and Bialek, J. (2022). Security constrained OPF utilizing substation reconfiguration and busbar splitting. *Electr. Power Syst. Res.* 212, 108507. doi:10.1016/j.epsr.2022.108507
- Nagi, F., Azwin, A., Boopalan, N., Ramasamy, A. K., Marsadek, M., and Ahmed, S. K. (2022). Comparison of grid reactive voltage regulation with reconfiguration network for electric vehicle penetration. *Electron. (Basel)* 11 (19), 3221. doi:10.3390/electronics11193221
- Nguyen, T.-T., Dao, T.-K., Nguyen, T.-T., and Nguyen, T.-D. (2022). An optimal microgrid operations planning using improved archimedes optimization algorithm. *IEEE Access* 10, 67940–67957. doi:10.1109/access.2022.3185737
- Pan, J.-S., Wang, H.-J., Nguyen, T.-T., Zou, F.-M., and Chu, S.-C. (2022). Dynamic reconfiguration of distribution network based on dynamic optimal period division and multi-group flight slime mould algorithm. *Electr. Power Syst. Res.* 208, 107925. doi:10.1016/j.epsr.2022.107925
- Parsadust, H., Hajiabadi, M. E., and Lotfi, H. (2025). Bi-level graph-based optimisation for distribution network reconfiguration and optimal placement of TCLBS and DC switches. *IET Gener. Transm. Distrib.* 19 (1), e70144. doi:10.1049/gtd.2.70144
- Pirouzi, S., Latify, M. A., and Yousefi, G. R. (2020). Conjugate active and reactive power management in a smart distribution network through electric vehicles: a mixed integer-linear programming model. *Sustain. Energy Grids Netw.* 22, 100344. doi:10.1016/j.segan.2020.100344
- Rajaram, R., Kumar, K. S., and Rajasekar, N. (2015). Power system reconfiguration in a radial distribution network for reducing losses and to improve voltage profile using modified plant growth simulation algorithm with distributed generation (DG). *Energy Rep.* 1, 116–122. doi:10.1016/j.egy.2015.03.002
- Raju, G., and Bijwe, P. R. (2008). An efficient algorithm for minimum loss reconfiguration of distribution system based on sensitivity and heuristics. *IEEE Trans. Power Syst.* 23 (3), 1280–1287. doi:10.1109/TPWRS.2008.926084
- Rao, R. S., Narasimham, S. V. L., Raju, M. R., and Rao, A. S. (2011). Optimal network reconfiguration of large-scale distribution system using harmony search algorithm. *IEEE Trans. Power Syst.* 26 (3), 1080–1088. doi:10.1109/TPWRS.2010.2076839
- Rao, Y., Cui, X., Zou, X., Ying, L., Tong, P., and Li, J. (2023). Research on distributed energy storage planning-scheduling strategy of regional power grid considering demand response. *Sustainability* 15 (19), 14540. doi:10.3390/su151914540
- Rawat, T., Niazi, K. R., Gupta, N., and Sharma, S. (2021). Multi-objective techno-economic operation of smart distribution network integrated with reactive power support of battery storage systems. *Sustain. Cities Soc.* 75, 103359. doi:10.1016/j.scs.2021.103359
- Reddy, A. V. S., and Reddy, M. D. (2016). Optimization of distribution network reconfiguration using dragonfly algorithm. *J. Elect. Eng.* 16 (4), 1–10.
- Saffar, A., Hooshmand, R., and Khodabakhshian, A. (2011). A new fuzzy optimal reconfiguration of distribution systems for loss reduction and load balancing using ant colony search-based algorithm. *Appl. Soft Comput.* 11 (5), 4021–4028. doi:10.1016/j.asoc.2011.03.003
- Sahoo, N. C., and Prasad, K. (2006). A fuzzy genetic approach for network reconfiguration to enhance voltage stability in radial distribution systems. *Energy Convers. Manage.* 47 (18–19), 3288–3306. doi:10.1016/j.enconman.2006.01.004
- Saw, B. K., Bohre, A. K., Thakkar, J., and Kolhe, M. L. (2023). Techno-economic and environmental based approach for planning of SDG and DSTATCOM with impact of network reconfiguration using APSO and TLBO. *Distributed Generation & Altern. Energy J.* 38 (05), 1585–1608. doi:10.13052/dgaej2156-3306.38510
- Sou, K. C., and Giron, K. (2022). “Joint renewable generation maximization and radial distribution network reconfiguration,” in *2022 IEEE PES innovative smart grid technologies - asia (ISGT Asia)*. doi:10.1109/ISGTAsia54193.2022.10003612
- Subramaniam, A., and Singh, L. R. S. R. (2023). Optimal planning and allocation of Plug-in hybrid electric vehicles charging stations using a novel hybrid optimization technique. *PLoS ONE* 18 (7), e0284421. doi:10.1371/journal.pone.0284421
- Swarnkar, A., Gupta, N., and Niazi, K. R. (2011). Adapted ant colony optimization for efficient reconfiguration of balanced and unbalanced distribution systems for loss minimization. *Swarm Evol. Comput.* 1 (3), 129–137. doi:10.1016/j.swevo.2011.05.004
- Taher, S. A., and Karimi, M. H. (2014). Optimal reconfiguration and DG allocation in balanced and unbalanced distribution systems. *Ain Shams Eng. J.* 5 (3), 735–749. doi:10.1016/j.asej.2014.03.009
- Taylor, J. A., and Hover, F. S. (2012). Convex models of distribution system reconfiguration. *IEEE Trans. Power Syst.* 27 (3), 1407–1413. doi:10.1109/TPWRS.2012.2184307
- Tran, T. T., Truong, K. H., and Vo, D. N. (2020). Stochastic fractal search algorithm for reconfiguration of distribution networks with distributed generations. *Ain Shams Eng. J.* 11 (2), 389–407. doi:10.1016/j.asej.2019.08.015
- Wu, G., Mallipeddi, R., and Suganthan, P. N. (2017). Problem definitions and evaluation criteria for the CEC 2017 competition on constrained real parameter optimization. China: National University of Defense Technology. Available online at: https://www.researchgate.net/publication/317228117_Problem_Definitions_and_Evaluation_Criteria_for_the_CEC_2017_Competition_and_Special_Session_on_Constrained_Single-Objective_Real-Parameter_Optimization.
- Wu, Y., Liu, J., Wang, L., An, Y., and Zhang, X. (2023). Distribution network reconfiguration using Chaotic particle swarm chicken swarm fusion optimization algorithm. *Energies* 16 (20), 7185. doi:10.3390/en16207185
- Yang, B., Zhang, X., Yu, T., Shu, H., and Fang, Z. (2017). Grouped grey wolf optimizer for maximum power point tracking of doubly-fed induction generator based wind turbine. *Energy Convers. Manag.* 133, 427–443. doi:10.1016/j.enconman.2016.10.062
- Yang, S., Zhang, G., Gao, J., and Yuan, J. (2023). Voltage management of distributed photovoltaic cluster connected to a distribution network. *J. Phys. Conf. Ser.* 2564 (1), 012017. doi:10.1088/1742-6596/2564/1/012017
- Youssef, K. H. (2021). Optimal routing of ring power distribution systems. *Electr. Power Syst. Res.* 199, 107392. doi:10.1016/j.epsr.2021.107392
- Zin, A. A. M., Ferdavani, A. K., Khairuddin, A. B., and Naeini, M. M. (2012). Reconfiguration of radial electrical distribution network through minimum-current circular-updating-mechanism method. *IEEE Trans. Power Syst.* 27 (2), 968–974. doi:10.1109/TPWRS.2011.2174258